

1 **Marine anoxia initiates giant sulfur-bacteria mat proliferation and associated changes in**
2 **benthic nitrogen, sulfur, and iron cycling in the Santa Barbara Basin, California**

3 **Borderland**

4 David J. Yousavich^{1*}, De'Marcus Robinson², Xuefeng Peng³, Sebastian J. E. Krause^{1,4}, Frank
5 Wenzhöfer^{5,6,7}, Felix Janssen^{5,6}, Na Liu⁸, Jonathan Tarn⁸, Frank Kinnaman⁸, David L. Valentine⁸,
6 Tina Treude^{1,2*}

7

8 ¹Department of Earth, Planetary, and Space Sciences, University of California Los Angeles, 595 Charles E.
9 Young Drive East, Los Angeles, CA 90095, USA

10 ²Department of Atmospheric and Oceanic Sciences, University of California Los Angeles, Math Science
11 Building, 520 Portola Plaza, Los Angeles, CA 90095, USA

12 ³School of Earth, Ocean, and Environment, University of South Carolina, 701 Sumter Street, EWS 617,
13 Columbia, SC 29208, USA

14 ⁴Earth Research Institute, 6832 Ellison Hall, University of California Santa Barbara, Ca 93106-3060

15 ⁵HGF-MPG Joint Research Group for Deep-Sea Ecology and Technology, Alfred-Wegener-Institute,
16 Helmholtz-Center for Polar and Marine Research, Am Handelshafen 12, 27570 Bremerhaven, Germany

17 ⁶HGF-MPG Joint Research Group for Deep-Sea Ecology and Technology, Max Planck Institute for Marine
18 Microbiology, Celsiusstrasse 1, 28359 Bremen, Germany

19 ⁷Department of Biology, DIAS, Nordcee and HADAL Centres, University of Southern Denmark, 5230 Odense
20 M, Denmark

21 ⁸Department of Earth Science and Marine Science Institute, University of California, Santa Barbara, CA
22 93106, USA

23

24 **Correspondence:** David Yousavich (yousavdj@ucla.edu), Tina Treude (ttreude@g.ucla.edu)

25 **Abstract**

26

27 The Santa Barbara Basin naturally experiences transient deoxygenation due to its unique
28 geological setting in the Southern California Borderland and seasonal changes in ocean currents.
29 Long-term measurements of the basin showed that anoxic events and subsequent nitrate
30 exhaustion in the bottom waters have been occurring more frequently and lasting longer over the
31 past decade. One characteristic of the Santa Barbara Basin is the seasonal development of
32 extensive mats of benthic nitrate-reducing sulfur-oxidizing bacteria, which are found at the
33 sediment-water interface when the basin's bottom waters reach anoxia but still provide some
34 nitrate. To assess the mat's impact on the benthic and pelagic redox environment, we collected
35 biogeochemical sediment and benthic flux data in November 2019, after anoxia developed in the
36 deepest waters of the basin and dissolved nitrate was depleted (down to 9.9 μM). We found that
37 the ~~development~~ of mats was associated with a shift from denitrification to dissimilatory nitrate
38 reduction to ammonium. The zone of sulfate reduction appeared near the sediment-water
39 interface in sediment hosting these ephemeral white mats. We found that an exhaustion of iron
40 oxides in the surface sediment was an additional prerequisite for mat proliferation. Our research
41 further suggests that cycles of deoxygenation and reoxygenation of the benthic environment
42 result in extremely high benthic fluxes of dissolved iron from the basin's sediment. This work
43 expands our understanding of nitrate-reducing sulfur-oxidizing mats and their role in sustaining
44 and potentially expanding marine anoxia.

Deleted: presence

46 **Introduction**

47

48 Naturally occurring low-oxygen waters in the ocean are commonly observed below the ocean's
49 mixed layer where respiration consumes oxygen faster than it is produced or ventilated. When
50 low oxygen conditions occur along the western continental shelf in regions susceptible to
51 upwelling events and/or undergoing eutrophication, organic matter remineralization can
52 frequently drive oxygen concentrations to hypoxic ($O_2 < 63 \mu\text{M}$) (Middelburg and Levin, 2009)
53 and/or anoxic levels ($O_2 < 3 \mu\text{M}$) (Fossing et al., 1995b; Canfield et al., 2010). These areas are
54 usually referred to as Oxygen Minimum Zones (OMZs). In the water column of OMZs, nitrogen
55 reduction becomes an important mechanism for organic matter remineralization (Ward et al.,
56 2009). OMZs within coastal basins that experience seasonal changes in upwelling can experience
57 anoxic and nitrate reducing conditions that extend to the benthic environment, especially when
58 high productivity and associated organic matter export coincide with seasonal patterns of
59 physical mixing. This fundamental change in the redox conditions at the sediment-water
60 interface encourages elevated rates of anaerobic microbial processes and can promote organic
61 matter preservation in the sediments (Middelburg and Levin, 2009; Treude, 2011), though a
62 recent study suggests a thin reactive surface layer can provide high rates of organic matter
63 degradation in anoxic environments (Van De Velde et al., 2023). Persistent anoxia in these
64 coastal OMZ can lead to huge releases of sulfide (up to $13.7 \text{ mmol m}^{-2} \text{ d}^{-1}$) and ammonium (up
65 to $21.2 \text{ mmol m}^{-2} \text{ d}^{-1}$) into the water column (Sommer et al., 2016).

66

67 The Santa Barbara Basin (SBB) is an example of one of these coastal OMZs that experiences
68 seasonal deoxygenation. Drastic changes in water column oxygenation and seafloor redox

Deleted: usually

Deleted: transformation such as through canonical denitrification or dissimilatory nitrate reduction to ammonium (DNRA) becomes is the dominant

Deleted: mechanism

Deleted: denitrifying

Deleted: (

Deleted: fluxes)

Deleted: in

Deleted: s

Deleted: ¶

The Santa Barbara Basin (SBB) is a coastal basin in the California Borderland with an approximate maximum depth of 600 m characterized by a seasonally anoxic water column (Sverdrup and Allen, 1939; Sholkovitz and Gieskes, 1971). The transform boundary along the California Borderland heavily affects the geomorphology of basins in this region; these basins become twisted as the plates rub against each other and form a series of "bathtubs" blocked by sills and seamounts off the coast of California. The SBB is bordered by the California coast in the north, the Channel Islands in the south, the Santa Monica basin to the east, and the Arguello Canyon to the west. A sill to the west of the basin at around 475 m depth (Fig. 1) prohibits most water transfer between the Santa Lucia Slope and the deeper waters of the SBB (Sholkovitz and Gieskes, 1971). The highly productive surface waters in the basin provide ample organic matter to the basin's water column, encouraging strong remineralization processes below the euphotic zone, which can induce anoxia below the sill depth, with typically less than $1 \mu\text{mol O}_2 \text{ L}^{-1}$ (Sholkovitz, 1973; Emery et al., 1962; Thunell, 1998; Emmer and Thunell, 2000). During upwelling events (usually in Spring), oxygenated waters from the California Current spill over the western sill and ventilate the SBB, increasing oxygen concentrations to approximately $20 \mu\text{mol O}_2 \text{ L}^{-1}$ (Goericke et al., 2015). SBB water-column oxygen and nitrogen concentrations have been evaluated through a longitudinal survey by the California Cooperative Oceanic Fisheries Investigations (Calcofi) with data starting in the 1950's. The data collected by this survey shows increasingly ubiquitous anoxia and denitrification in the basin with the SBB becoming completely nitrate-depleted below the sill at least three times between 2012 and 2017 (<https://calcofi.org/data/>).¶

Deleted: These d

Deleted: SBB

115 conditions drive complex changes in benthic biogeochemistry and microbiology, evidenced most
 116 clearly by the development of thick, expansive mats of giant sulfur-oxidizing bacteria (GSOB)
 117 on the SBB seafloor (Bernhard et al., 2003; Prokopenko et al., 2006; Valentine et al., 2016;
 118 Kuwabara et al., 1999). A 2016 survey of the basin identified a vast GSOB mat spread over 1.6
 119 contiguous km, confined between 487 and 523 km in the SBB depocenter where conditions were
 120 anoxic but not depleted of NO_3^- (Valentine et al., 2016). These GSOB mats have been noted
 121 previously in the SBB benthos, appearing at times of anoxia and disappearing when oxygen is
 122 present in the bottom water (Reimers et al., 1996b; Kuwabara et al., 1999). Similar GSOB mats
 123 have been identified in other transiently deoxygenated OMZs such as the Peruvian/Chilean coast
 124 (Sommer et al., 2016; Schulz et al., 1996; Zopfi et al., 2001; Høglund et al., 2009). The
 125 chemoautotrophic bacteria that constitute the bulk of GSOB mats (typically *Thioploca* and/or
 126 *Beggiatoa*) utilize sulfide as an electron donor and O_2 or NO_3^- as a terminal electron acceptor
 127 (Jørgensen and Nelson, 2004). Some GSOB can hyperaccumulate NO_3^- in cell vacuoles up to
 128 500 mM (Fossing et al., 1995a) and use this NO_3^- reserve to oxidize sulfide that diffuses from the
 129 underlying sediment to perform their metabolism. (Huettel et al., 1996; Mußmann et al., 2003;
 130 Sayama, 2001).

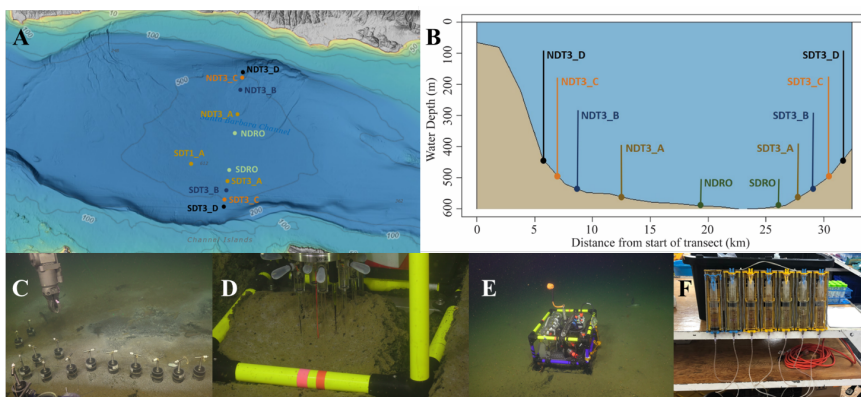
Deleted: mats

Deleted: at

Deleted: seafloor

Deleted:

Deleted: including



131

137
138
139
140
141
142
143
144
145
146
147
148
149
150
151
152
153
154
155
156
157
158
159
160
161
162

Figure 1. Maps of sampling locations in the Santa Barbara Basin and photographs of deployed equipment: (A) bathymetric map of the Santa Barbara Basin with locations of all sampled stations; (B) cross-section of the Santa Barbara Basin with locations of all sampled station; (C) sediment push coring with ROV arm; (D) sediment microprofiler; (E) benthic flux chamber; (F) closeup of a syringe system from a benthic flux chamber. The map in (A) was generated using the Bathymetric Data Viewer provided by the National Centers for Environmental Information.

The activity of GSOB mats contribute significantly to element cycling in benthic marine environments with large effects on biogeochemical conditions in the bottom water. Isotopic measurements of $^{15}\text{N}/^{14}\text{N}$ and $^{18}\text{O}/^{16}\text{O}$ from NO_3^- in the SBB water column suggest that benthic organisms are responsible for approximately 75% of the total NO_3^- reduction in the SBB (Sigman et al., 2003). Other studies found that GSOB mats inhibit the diffusion of NO_3^- into sediments via hyper-accumulation in vacuoles thereby creating conditions ideal for bacterial heterotrophic sulfate reduction beneath them (Fossing et al., 1995b; Zopfi et al., 2001). These studies suggest that GSOB mats in the SBB may be responsible for the majority of NO_3^- consumption in the basin rather than water-column microbes. Additionally, GSOB mats have been reported to deplete NO_3^- via dissimilatory nitrate reduction to ammonia (DNRA) in the anoxic bottom water of the Peruvian OMZ (Dale et al., 2016) and in the hypoxic transition zone in the Eastern Gotland Basin of the Baltic Sea (Noffke et al., 2016). By contrast, benthic microbial communities in the hypoxic (42 μM) Mauritanian OMZ perform canonical denitrification instead (Dale et al., 2014). The contrast between the Peruvian and Mauritanian OMZ suggests that bottom-water anoxia triggers the appearance of GSOB mats, and that DNRA is more prevalent where GSOB mats are present.

- Deleted: These GSOB mats are ephemeral in the SBB, appearing to proliferate and potentially migrate depending on bottom water oxidant concentrations (Kuwabara et al., 1999).
- Deleted: in turn
- Deleted: the SBB
- Deleted: sedimentary
- Deleted: uptake
- Deleted: organoclastic
- Deleted: D
- Deleted: N
- Deleted: R
- Deleted: Ammonium
- Deleted: .
- Deleted: (two coastal upwelling zones similar to the SBB)
- Deleted:

178 The rapid accumulation and consumption of NO_3^- by GSOB mats has ramifications for the redox
179 conditions in the sediment underneath. The depletion of NO_3^- and shallowing of the nitracline
180 could promote high rates of sulfate reduction in the sediment underneath the GSOB mat. In
181 return, the sulfate reduction zone exists close to the sediment-water interface, providing the
182 GSOB mat with readily accessible sulfide. If a metabolic feedback loop is then established
183 between sulfur-oxidizing bacteria at the sediment-water interface and sulfate-reducing bacteria in
184 the sediment, increased NO_3^- loss from the water column and spreading of sulfidic conditions in
185 SBB sediment is expected. With these mats being potentially crucial to nitrogen and sulfur
186 cycling in sediments underlying OMZs, their biogeochemical transformations and ergo effect
187 upon basin redox conditions are critically important to understanding element cycling in the
188 SBB. Such gained knowledge would have additional benefits for predicting biogeochemical
189 feedbacks to the projected expansion of oceanic oxygen deficiency, in the SBB and in OMZs
190 more general, as a result of global change (Stramma et al., 2008).

191
192 Utilizing in-situ technologies, sediment porewater extraction, solid phase analyses, and
193 radiotracer techniques, this study aims to answer the following overarching questions: (1) Which
194 environmental conditions initiate and sustain the proliferation of GSOB mats? (2) Which
195 biogeochemical transformations occur in the sediment underneath these mats? (3) What role do
196 the mats play in the increasingly prevalent anoxic and nitrate-depleted condition found in the
197 SBB? These investigations represent the first basin-wide geochemical characterization of the
198 Santa Barbara Basin which hosts the largest as-of-yet mapped GSOB mat in the world's oceans.
199 It is the first suite of in-situ flux measurements carried out in the SBB, which is unique to other
200 heavily studied marine settings (e.g., Eastern Gotland Basin, Peruvian upwelling zone) in that it

201 is an oceanic basin within an upwelling zone. The results presented here also provide
202 geochemical context for a number of other related investigations in the SBB (Robinson et al.,
203 2022; Peng et al., 2023) as well as the first measurements in a multi-year study of
204 biogeochemical changes in response to warming waters and increased stratification on the
205 California coast.

206 **2. Materials and Methods**

207 **2.1 Study Site**

208 The Santa Barbara Basin (SBB) is a coastal basin in the California Borderland with an
209 approximate maximum depth of 600 m characterized by a seasonally anoxic water column
210 (Sverdrup and Allen, 1939; Sholkovitz and Gieskes, 1971). The transform boundary along the
211 California Borderland heavily affects the geomorphology of basins in this region; these basins
212 become twisted as the plates rub against each other and form a series of “bathtubs” blocked by
213 sills and seamounts off the coast of California. The SBB is bordered by the California coast in
214 the north, the Channel Islands in the south, the Santa Monica basin to the east, and the Arguello
215 Canyon to the west. A sill to the west of the basin at around 475 m depth (Fig. 1) prohibits most
216 water transfer between the Santa Lucia Slope and the deeper waters of the SBB (Sholkovitz and
217 Gieskes, 1971). The highly productive surface waters in the basin provide ample organic matter
218 to the basin’s water column, encouraging strong remineralization processes below the euphotic
219 zone, which can induce anoxia below the sill depth, with typically less than 1 $\mu\text{mol O}_2 \text{L}^{-1}$
220 (Sholkovitz, 1973; Emery et al., 1962; Thunell, 1998; Emmer and Thunell, 2000). Benthic faunal
221 distribution within the basin is tightly correlated with this sill depth and related oxygen
222 conditions; below the sill, the sea snail *Alia permodesta* is the most commonly found benthic
223 fauna, while sea stars, sea urchins, and other echinoderms increase in density above the sill
224 (Myhre et al., 2018). During upwelling events (usually in Spring), oxygenated waters from the
225 California Current spill over the western sill and ventilate the SBB, reportedly increase bottom
226 water oxygen concentrations to approximately 20 $\mu\text{mol O}_2 \text{L}^{-1}$ (Goericke et al., 2015). SBB
227 water-column oxygen and nitrogen concentrations have been evaluated through a longitudinal
228 survey by the California Cooperative Oceanic Fisheries Investigations (Calcofi) with data

Deleted: ¶

Deleted: F

231 ~~starting in the 1950's . The data collected by this survey shows increasing durations of anoxia~~
232 ~~and fixed nitrogen loss in the basin with the SBB becoming completely nitrate-depleted below~~
233 ~~the sill at least three times between 2012 and 2017 (<https://calcof.iorg/data/>).~~

Deleted: ly ubiquitous

235 **2.2 Benthic sediment sampling and instrument deployment**

Deleted: 1

236 Sediment samples were taken between 30 October and 11 November 2019 during an expedition
237 aboard the research vessel (*R/V Atlantis*) equipped with the remote operated vehicle (ROV)
238 Jason. Samples were taken at stations along a bimodal, north-south transect through the
239 depocenter of the SBB, as well as one station on a separate transect. Details of sampling stations
240 can be seen in Fig. 1A and 1B. Briefly, depocenter stations are labeled as NDRO and SDRO
241 (northern and southern depocenter radial origin, respectively). The remaining stations are named
242 for the cardinal direction (north vs. south) and the transect number (e.g., SDT1-A is on transect 1
243 while SDT3-A is on transect 3). As station depth decreases, the alpha suffix increases (e.g.,
244 NDT3-A is deeper than NDT3-B, etc.).

246 ROV Jason conducted sediment push coring and deployed automated benthic flux chambers
247 (BFC) and microprofilers at each station. ~~Bottom water oxygen concentration was determined~~
248 ~~using an Aanderaa 4831 oxygen optode (Aanderaa Instruments, Bergen, Norway) installed on~~
249 ~~the ROV. Optical modems (Luma 250LP, Hydromea, Renens, Switzerland) installed on the ROV~~
250 ~~and the BFC and microprofilers~~ were used to transmit deployment settings and ~~start/terminate~~
251 ~~measurements of the instruments~~. Multiple push cores (polycarbonate, 30.5 cm length, 6.35 cm
252 inner diameter) per sampling station were retrieved during ROV Jason deployments (Fig. 1C).
253 ~~Replicate cores from each station were transferred to an onboard 6°C cold room upon recovery~~

Deleted: Station depth, latitude, and longitude were automatically generated by the Jason data processor using navigation data derived from the Doppler Velocity Log system and the ultrashort baseline positioning system.

Deleted: initiate

Deleted: communications

Deleted: between ROV Jason and the BFC/microprofilers

Deleted: These cores were inserted into the sediment and retrieved using Jason's manipulator arm. Cores were then stored in a 6-core capacity basket and transported to the surface using a free-ascending underwater elevator.

Deleted: immediately

Deleted: arrival at the

269 ~~aboard the ship~~ and subsampled for either solid phase analyses, porewater geochemistry, or
270 radiotracer experiments.

Deleted: (representing average in-situ temperature)

271

272 2.3 Sediment Core Sub-Sampling

Deleted: 2

273 ~~Two replicate ROV push cores that were collected near each other at each station~~ were processed
274 under a constant argon flow to protect redox-sensitive species. Cores were sectioned in 1-cm

Deleted: For sediment porewater geochemistry analyses, t

Deleted: that

Deleted: and

275 increments up to 10 cm followed by 2-cm increments. Note, sediments from the NDT3-B station

Deleted: below 10 cm

276 were sliced in 2-cm increments. Sediment subsections were transferred into argon-filled 50-mL

277 conical centrifuge tubes. ~~Sediment samples were centrifuged at 2300 x g for 20 minutes. The~~

Deleted: Porewater was retrieved after

Deleted: s

278 ~~centrifugate was subsampled unfiltered as fast as possible (to avoid contaminations with oxygen)~~

Deleted: and

Deleted: t

279 ~~for porewater analyses~~. Solid phase cores were sectioned similar to porewater cores and sub-

Deleted: left

280 sampled for sediment density, porosity, and organic matter content. A 10 mL cut-off plastic

Deleted: and

Deleted: analyses

281 syringe was used to collect 6 mL of sediment into pre-weighed plastic vials (15 mL snap-cap

282 vials) and stored in the dark at 4°C for sediment porosity and density analysis. Two-mL

283 microcentrifuge tubes were filled with sediment from each depth interval and stored at -30°C for

284 sediment organic matter analyses. One ROV push core per station was sub-sampled with a

285 miniaturized push core (length 20 cm, inner diameter 2.6 cm) and taken immediately to the

286 shipboard radioisotope van for radiotracer experiments (see section 2.5).

287

288 2.4 Sediment Porewater Geochemistry

Deleted: 3

289 Concentrations of porewater sulfide (Cline, 1969), NH_4^+ , PO_4^{3-} , and Fe^{2+} (Grasshoff et al., 1999)

Deleted: Geochemical analyses were performed to provide context for electron donors and acceptors of benthic microbial metabolisms, sediment redox states, and organic matter degradation. ...

290 were determined shipboard with a Shimadzu UV-Spectrophotometer (UV-1800). Detection

Deleted: from the unfiltered porewater

291 limits for sulfide, NH_4^+ , PO_4^{3-} , and Fe^{2+} were 1 μM . Subsamples (2 mL) for porewater NO_3^- and

311 NO₂⁻ concentrations were stored in 2-mL plastic vials with an O-ring, frozen shipboard at -30°C
312 and analyzed back at the home laboratory, on the same spectrophotometer using the method
313 following (García-Robledo et al., 2014). The detection limit for NO₃⁻ and NO₂⁻ was 0.5 µM.
314 Samples for porewater DIC were preserved shipboard with 5 µL saturated HgCl in headspace
315 free glass vials and stored at 4°C for later analysis following (Hall and Aller, 1992). DIC
316 detection limit was 0.1 mM. Total alkalinity was determined shipboard using direct titration of
317 500 µL of pore water with 0.01M Titrisol® HCl (Pavlova et al., 2008). The analysis was
318 calibrated using IAPSO seawater standard, with a precision and detection limit of 0.05 meq L⁻¹.
319 Subsamples (1 mL) for sulfate and chlorinity were stored in 2-mL plastic vials with an O-ring,
320 frozen shipboard at -30°C and later measured in the lab using a Metrohm 761 ion chromatograph
321 with a methodological detection limit of 30 µM (Dale et al., 2015).

Deleted: in the lab

Deleted: 5

323 2.5 Solid Phase Analyses

324 Porosity/Density samples were collected in pre-weighed plastic vials and dried at 50°C for up to
325 96 hr until the dry weight was stable. Sediment porosity was calculated by taking the difference
326 between wet and dry sediment weight and divided by the volume of the wet sediment. Sediment
327 density was calculated by dividing the wet sediment weight by its volume. Treatment of
328 sediment subsamples for total organic carbon (TOC), total organic nitrogen (TON), and organic
329 carbon isotope composition (δ¹³C) were modified from (Harris et al., 2001) and sent to the
330 University of California Davis Stable Isotope Facility for analysis using Elemental Analyzer –
331 Isotope Ratio Mass Spectrometry. TOC and TON were calculated based on the sample peak area
332 corrected against a reference material (alfalfa flour). Limit of quantification based on peak area
333 was 100 µg C with an uncertainty of ± 0.2 % for δ¹³C.

Deleted: 4

Deleted: Plastic vials for sediment porosity and density measurements were weighed prior to the expedition.

Deleted: S

Deleted: the

Deleted: were

Deleted: determined by calculating

Deleted: determined

Deleted: Analyses

Deleted: for

Deleted: .

Deleted: Briefly, samples were dried up to 48 hours at 50°C until the dry weight was stable and then treated with direct addition of 1 mL of 6N HCl to dissolve carbonate minerals. These samples were then washed in triplicate with 1-mL of ultrapure water or until a neutral pH was re-established. Samples were centrifuged at 4255 x g for 20 minutes, the supernatant was decanted, and vials were re-dried at 50°C. A subsample (approximately 10-15 mg of sediment) was then packed into individual 8x5 mm pressed tin capsules

356

357 2.6 Sulfate Reduction

358 To determine ex-situ microbial sulfate reduction rates, whole round sub-cores were injected with
359 10 μL carrier-free ^{35}S -Sulfate radiotracer (dissolved in water, 200 kBq, specific activity 37 TBq
360 mmol^{-1}) into pre-drilled, silicon-filled holes at 1-cm increments according to (Jørgensen, 1978).

361 These sub-cores were incubated at 6°C in the dark for 6-8 hours. Incubations were stopped by
362 slicing sediment cores in 1-cm increments into 50-mL centrifuge tubes filled with 20-mL zinc

363 acetate (20% w/w) and frozen at -20°C until analysis at the land-based laboratory. Microbial
364 activity in controls was terminated with zinc acetate (20 mL of 20% w/w) before the addition of
365 radiotracer and subsequent freezing. Lab-based analysis of sulfate reduction rates were
366 determined following the cold-chromium distillation procedure (Kallmeyer et al., 2004).

368 2.7 Benthic In-Situ Investigations

369 Per station, one to three microprofiler (Fig. 1D) and three BFC (Fig. 1E) deployments were
370 carried out by the ROV Jason at the seafloor. Construction, deployment and operation of
371 automated microprofilers and BFCs followed those described in (Treude et al., 2009). The

372 microprofiler deployed in this study represents a modified, miniaturized version of the
373 instrument described in (Gundersen and Jørgensen, 1990) that was constructed specifically for
374 use by ROV. Microprofilers were outfitted with three O_2 -microelectrodes (Glud et al., 2000),
375 two pH-microelectrodes (Revsbech and Jørgensen, 1986), two H_2S -microelectrodes
376 (Jeroschewsky et al., 1996), and one conductivity sensor to determine the position of the
377 sediment-water interface relative to the tips of the microelectrodes. Concentrations of oxygen

Deleted: 5

Deleted: Triplicate "killed" controls were produced using homogenized sediment from the same ROV push core.

Deleted: Sulfate reduction rates were calculated per volume of wet sediment (cm^3) following equation:

$$SRR = [SO_4] * P_{SED} * \frac{a_{TRIS}}{a_{TOT}} * \frac{1}{t} * 1.06 * 1000$$

(EQ # 1)

Where SRR is sulfate reduction rate ($\text{nmol cm}^{-3} \text{d}^{-1}$); $[SO_4]$ is porewater sulfate concentration; P_{SED} is sediment porosity; a_{TRIS} is radioactivity of the total reducible inorganic sulfur (counts per minute); a_{TOT} is total radioactivity used in incubation (counts per minute); t is incubation time in days; 1.06 is the correction factor for expected isotope fractionation; and 1000 is the factor to convert from mmol L^{-1} to nmol cm^{-3} .

Deleted: 6

Deleted: rc

397 and sulfide, as well as pH were each calculated from microelectrode readings ~~and averaged for~~
398 ~~the respective sites~~ where replicates existed.

Deleted: as an

Deleted: per

Deleted: Microprofiler frames (and benthic flux chamber frames) were outfitted with syntactic foam to reduce the negative buoyancy of the instruments in water and prevent them from sinking into the extremely soft sediments in the SBB. ...

399
400 The BFC consisted of a frame equipped with a cylindrical polycarbonate chamber (inner
401 diameter = 19 cm) with its lower portion sticking out of the frame. The upper side of the
402 chamber was closed by a lid containing a stirrer (Type K/MT 11, K.U.M., Kiel, Germany),
403 oxygen optodes (Type 4330, Aanderaa Data Instruments, Bergen Norway and Hydroflash,
404 Contros/Kongsberg Maritime, Kongsberg, Norway), a conductivity sensor (type 5860, Aanderaa
405 Data Instruments), and a valve. Prior to insertion into the sediments, the chambers were held
406 upside down by the ROV manipulating arms within approximately 10 m of the seafloor and
407 moved back and forth to make sure that water from shallower depth that may have been trapped
408 was replaced by bottom water. Chamber incubations lasted between 240 and 390 minutes. Each
409 BFC was outfitted with a custom-built syringe sampler containing seven syringes that were
410 connected by tubes to sampling ports in the upper wall of the chambers (Fig. 1F): one injection
411 syringe and six sampling syringes that were fired at regular time intervals over the time course of
412 the deployment. The injection syringe contained de-ionized water and the reduction in salinity in
413 the overlaying water after salinity readings stabilized (i.e., full mixing was achieved) 10-30 min
414 after injection was used to determine BFC volumes (Kononets et al., 2021). Samples obtained
415 from the overlaying water of the BFC were examined for the same geochemical constituents as
416 described above (section 2.4). Benthic fluxes of NO_3^- , NH_4^+ , PO_4^{3-} , and Fe^{2+} were calculated as
417 follows:

418

419
$$J = \frac{\Delta c}{\Delta t} * \frac{V}{A} \quad (\text{EQ \# 2})$$

427

428 Where J is the flux in $\text{mmol m}^{-2} \text{d}^{-1}$, ΔC is the concentration change in mmol m^{-3} , Δt is the time
429 interval in d, V is the overlying water volume in m^3 , and A is the surface area of the sediment
430 covered by the benthic flux chamber in m^2 . ~~An average flux within BFC's was calculated for~~
431 stations of similar depth. One chamber per site contained $^{15}\text{N-NO}_3^-$ in the injection syringe for in-
432 situ nitrogen cycling experiments. Results are reported from two of these chambers (SDRO and
433 NDT3-D) and all $^{15}\text{N-NO}_3^-$ chambers were excluded from benthic flux calculations (see next
434 section).

435

436 **2.8 In Situ ^{15}N Incubations**

437 Two hundred μmol of ^{15}N -labeled potassium nitrate (99% ^{15}N ; Cambridge Isotopes) was injected
438 into the ^{15}N incubation chamber at each site to obtain a final concentration of $\sim 50 - 100 \mu\text{M}$ ^{15}N -
439 labeled nitrate. Nitrate was amended at this level to prevent its depletion before the last sampling
440 time point (Valentine et al., 2016). Samples for $\delta^{15}\text{N}$ analysis were preserved by filling a pre-
441 vacuumed 12-ml exetainer vial with 0.1 ml 7M zinc chloride as a preservative. Another aliquot
442 (~ 12 ml) of seawater for ammonium isotope analysis (see section 2.7.2) was filtered through 0.2
443 μm syringe filters and stored frozen. Prior to analyzing the samples in 12-ml exetainer vials, 5
444 mL of sample was replaced with ultra-high purity helium to create a headspace. The
445 concentration and $\delta^{15}\text{N}$ of dissolved N_2 and N_2O was determined using a Sercon CryoPrep gas
446 concentration system interfaced to a Sercon 20-20 isotope-ratio mass spectrometer (IRMS) at the
447 University of California Davis Stable Isotope Facility.

448

449 **2.9 Ammonium Isotope Analyses**

Deleted: diffusive

Deleted: Final diffusive

Deleted: as

Deleted: averaged

Deleted: (e.g., we averaged calculated diffusive flux from NDT3-A and SDT3-A and report as "A stations").

Deleted: 7.1

Deleted: 7.2

458 The production of $^{15}\text{NH}_4^+$ in seawater samples was measured using a method adapted from
459 (Zhang et al., 2007) and described previously by (Peng et al., 2016). In brief, NH_4^+ was first
460 oxidized to NO_2^- using hypobromite (BrO^-) and then reduced to N_2O using an acetic acid-azide
461 working solution (Zhang et al., 2007). The $\delta^{15}\text{N}$ of the produced N_2O was determined using an
462 Elementar Americas PrecisiON continuous flow, multicollector, isotope-ratio mass spectrometer
463 coupled to an automated gas extraction system as described in (Charoenpong et al., 2014).
464 Calibration and correction were performed as described in (Bourbonnais et al., 2017). The
465 measurement precision was ± 0.2 ‰ for $\delta^{15}\text{N}$. Depending on the in-situ ammonium
466 concentration, the detection limit for total NH_4^+ production rates ranged between 0.006 and
467 $0.0685 \text{ mmol m}^{-2} \text{ d}^{-1}$.

468

469 **3. Results**

470 **3.1 Bottom water conditions**

471 O_2 and NO_3^- concentrations in the bottom water along the transects can be seen in Table 1. O_2
472 concentrations below detection as determined by the ROV sensor could in some cases be
473 considered to represent anoxia ($0 \mu M O_2$) based on a set of different analytical methods (see
474 discussion section 4.1). Bottom water solute concentrations (as defined by the average T_0
475 concentration in BFC at each site) can be seen in Suppl. Figs. 1-4. Bottom water NO_3^-
476 concentrations roughly decreased with station depth (e.g., $28 \mu M$ at NDT3-D vs. $19 \mu M$ at
477 NDRO). Bottom water NO_2^- concentrations were below detection at all stations. Bottom water
478 NH_4^+ concentrations were $9 \mu M$ at NDRO and $13 \mu M$ at SDRO and below detection in shallower
479 stations. Bottom water PO_4^{3-} concentrations roughly increased with increasing basin depth (e.g.,
480 $2 \mu M$ at SDT3-D vs. $7 \mu M$ at SDRO). Finally, Fe^{2+} was 2 and $5 \mu M$ at the NDRO and SDRO
481 stations, respectively and below detection at all shallower stations.

483 **3.2 Sediment characteristics**

484 Photographs of sediment cores with a depth scale are shown below Table 1. Sediment colors
485 were classified according to (Hossain et al., 2014). Cores from the shallowest (D) stations were
486 uniformly reddish in color with small pockets of black. The sediment color changed with station
487 depth, transitioning from a reddish color in the shallowest stations to predominantly black with
488 reddish laminations at the depocenter stations. The band of black sediment appeared at approx. 8
489 cm sediment depth in the C-station cores and became progressively more ubiquitous with station
490 depth. Notably, NDT3-C sediment (Table 1B) contained black bands from approx. 6-14 cm
491 sediment depth, while SDT3-C sediment (Table 1J) had a much narrower band around 8-10 cm.

Deleted: , i.e., in the water surrounding the ROV during its operations at the seafloor and in the benthic flux chambers at T_0 , respectively,

Deleted: O_2 concentration roughly decreased with increasing basin depth, $10 \mu M O_2$ at SDT3-D vs. ($<3 \mu M O_2$) at SDRO)

Deleted: time 0

Deleted: ,

Deleted: , respectively

Deleted: showed similar trends to NH_4^+

Deleted: , with an average concentration of 1 and

Deleted: NDT3-D and

Deleted: stations, respectively,

Deleted: and

Deleted: 5 and

Deleted: NDRO and

Deleted:

Deleted: stations, respectively

Deleted: . Bottom water Fe^{2+} was

Moved (insertion) [3]

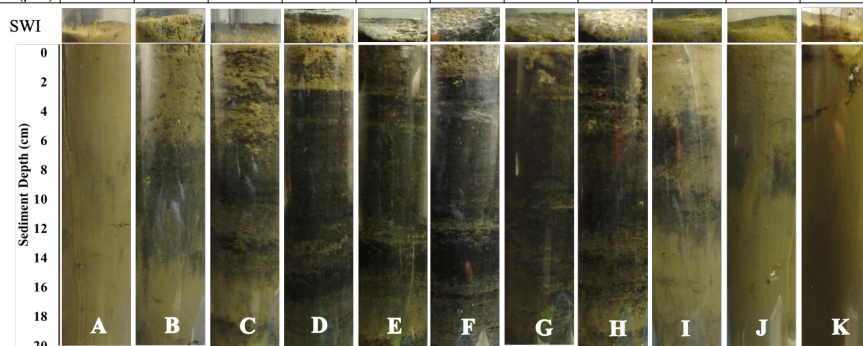
Deleted: exhibited iron sulfide formation

511 Sediment cores from shallower stations (D and C stations) contained signs of bioturbation (e.g.,
 512 u-shaped burrows) and, in some cases, contained visible macrofauna, such as polychaetas and
 513 mollusks. Deeper in the basin (A and depocenter stations) no signs of bioturbation were detected,
 514

Deleted: (the same depth at which Fe²⁺ concentrations decrease in the porewater).

515 **Table 1.** Station details and photos of representative ROV push cores taken at each station. Mat presence (Y =
 516 yes, N = no) was determined visually. Station water depth and oxygen concentration were determined by sensors
 517 attached to ROV Jason (bdl = below detection limit (<3 μM O₂)). Anoxia was confirmed by additional methods
 518 (see discussion section 4.1). Latitude and longitude were determined by triangulation between the ROV and the
 519 ship. Bottom water nitrate concentration was derived from an average of benthic flux chamber nitrate
 520 measurements at time 0 for each station (chambers with no calculatable flux and ¹⁵N-nitrate addition excluded).
 521 Note, benthic flux chambers were not deployed at SDT1-A. Photographs show the sediment-water interface
 522 (SWI; top part) and each sediment core in full length (lower part).
 523

Parameter	NDT3-D	NDT3-C	NDT3-B	NDT3-A	NDRO	SDRO	SDT1-A	SDT3-A	SDT3-B	SDT3-C	SDT3-D
Mat Present	N	N	N	Y	Y	Y	Y	Y	N	N	N
Depth (m)	447	498	537	572	580	586	573	571	536	494	447
Latitude (°)	34.363	34.353	34.333	34.292	34.262	34.201	34.212	34.184	34.168	34.152	34.142
Longitude (°)	-120.015	-120.016	-120.019	-120.026	-120.031	-120.044	-120.116	-120.047	-120.053	-120.050	-120.052
Oxygen (μM)	8.7	5.2	12.2	9.2	0.0	0.0	0.0	0.0	1.8	3.1	9.6
Nitrate (μM)	27.3	26.0	11.5	24.4	18.5	9.9		20.4	20.6	16.3	28.0



524
 525
 526 and the sediment-water interface was colonized by patches of white GSOB mats. Spherical cells
 527 (given the moniker ‘ghost balls’) were found mixed amongst giant sulfur bacteria filaments
 528 within the top 0-1 cm of sediment at NDRO (Suppl. Fig. 7). These unknown species had similar
 529 morphological characteristics to the species *Thiomargarita namibiensis* (Schulz et al., 1999;
 530 Schulz and Schulz, 2005) containing a translucent cell with sulfur granules giving them a ghostly

Deleted: d,

Deleted: 5

535 white appearance. A small sample of cells ($n = 8$) were measured, featuring diameters between
 536 48.0 and 99.6 μm , amounting to an average biovolume of $2.5 \times 10^5 \mu\text{m}^3$, compared to *T.*
 537 *namibiensis* with a cell diameter usually between 100-300 μm (Schulz et al., 1999).

Deleted: up to 700 μm

538
 539 **Table 2.** Sediment solid phase data: porosity, density, total organic carbon (TOC), total organic nitrogen (TON),
 540 C:N ratio, and $\delta^{13}\text{C}$. All data were averaged for the top 0-19 cm sediment, except NDT3-C (17 cm), NDT3-A
 541 (11 cm) and SDRO (7 cm), where the core length was shorter. Integrated sulfate reduction rates (iSRR) were
 542 integrated over 0-14 cm sediment depth. No sulfate reduction rates are available for NDT3-B, SDT3-A, and
 543 SDT3-B; rates were not integrated for SDRO due to missing surface samples.

Parameter	NDT3-D	NDT3-C	NDT3-B	NDT3-A	NDRO	SDRO	SDT1-A	SDT3-A	SDT3-B	SDT3-C	SDT3-D
Porosity	0.79 ± 0.03	0.81 ± 0.04	0.86 ± 0.04	0.88 ± 0.03	0.88 ± 0.04	0.87 ± 0.03	0.88 ± 0.03	0.86 ± 0.04	0.85 ± 0.04	0.82 ± 0.04	0.78 ± 0.04
Density	1.21 ± 0.07	1.16 ± 0.08	1.06 ± 0.08	1.05 ± 0.04	1.06 ± 0.03	1.04 ± 0.03	1.11 ± 0.23	1.05 ± 0.05	1.12 ± 0.06	1.22 ± 0.05	1.22 ± 0.03
TOC (%)	2.9 ± 0.5	2.5 ± 0.5	3.6 ± 0.5	3.1 ± 0.4	3.3 ± 0.4	3.5 ± 0.4	4.5 ± 0.5	3.2 ± 0.0	3.6 ± 0.6	3.6 ± 0.8	3.3 ± 0.5
TON (%)	0.3 ± 0.1	0.5 ± 0.1	0.4 ± 0.1	0.4 ± 0.1	0.4 ± 0.0	0.4 ± 0.1	1.0 ± 0.1	0.4 ± 0.0	0.4 ± 0.1	0.4 ± 0.1	0.4 ± 0.1
C:N Ratio	8.9 ± 0.2	8.7 ± 0.5	8.5 ± 0.5	8.2 ± 0.2	8.2 ± 0.4	8.0 ± 0.2	8.6 ± 0.8	8.3 ± 0.6	8.3 ± 0.3	8.7 ± 0.3	8.5 ± 0.2
$\delta^{13}\text{C}$ (‰)	-22.4 ± 0.3	-22.4 ± 0.4	-22.2 ± 0.4	-22.1 ± 0.2	-22.1 ± 0.2	-22.0 ± 0.3	-21.3 ± 0.7	-22.1 ± 0.4	-22.0 ± 0.2	-21.9 ± 0.2	-22.0 ± 0.1
Integrated SRR (mmol m ⁻² d ⁻²)	2.9	3.8		2.7	4.1		2.9			1.7	1.9

545
 546
 547
 548 B station cores contained sporadic GSOB filaments slightly deeper in the sediment (approx. 2-4
 549 cm sediment depth). Sediment solid phase parameters (averaged over the entire sediment core
 550 depth) can be seen in Table 2. Average sediment porosity increased with basin depth (e.g., from
 551 0.79 at NDT3-D to 0.88 at NDRO). TOC, TON, the C/N ratio, and the $\delta^{13}\text{C}$ isotopic signature of
 552 organic carbon remained relatively constant (2.5 – 4.5%, 0.1 – 0.4%, 8.0 – 8.7 and 21.3 –
 553 22.4 ‰, respectively) over all stations.

Deleted: Depocenter and A-station sediment was laminated throughout the entire core length, B-station sediment showed some lamination below the first 4 cm, but sediment from shallower stations had little (C station) to no signs of lamination (D station).

Deleted: and

555 3.3 Sediment porewater geochemistry

556 Total alkalinity (Figs. 2 A-E & 3 A-F) increased steadily with sediment depth at all stations
 557 starting with, on average, 2.4 mM in the core supernatant reaching a maximum at the respective
 558 deepest sediment sample (20 cm). Porewater alkalinity and DIC also increased with basin depth.

Deleted: Geochemical parameters of sediment porewater are shown in Fig. 2 (northern stations) and 3 (southern stations).

Deleted: Total

Deleted: ; cores in the depocenter exhibited higher total alkalinity (max. 9.6 mM at NDRO) than D-stations (max. 3.4 mM at NDT3-D). Porewater DIC

572 (Figs. 2 A-E & 3 A-F), indicating that total alkalinity was dominated by the carbonate system.

573 Porewater DIC was, on average, 2.2 mM in the core supernatant and reached maximum

574 concentrations at the deepest sediment depth (20 cm) at most stations. ▼

575

576 Porewater PO_4^{3-} profiles (Figs. 2 A-E & 3 A-F) were markedly different between the depocenter

577 and shallower C and D stations. Porewater PO_4^{3-} concentrations in the depocenter and A stations

578 generally increased with sediment depth but several profiles (NDT3-C, NDT3-A, SDRO, SDT1-

579 A) remained unchanged or decreased deeper in the sediment (starting at approx. 10 cm). The

580 profiles in C and D stations showed a peak in PO_4^{3-} concentrations near the sediment-water

581 interface, particularly in the northern basin. Below 2 cm, PO_4^{3-} decreased with sediment depth,

582 but sometimes showed a second small peak deeper in the sediment (12-14 cm at NDT3-D and

583 10-12 cm at SDT3-D).

584

585 Porewater NH_4^+ concentrations (Figs 2 & 3 A-E) showed trends often similar to alkalinity and

586 DIC; NH_4^+ concentrations increased downcore and were higher at depocenter than at D stations

587 (e.g., 370 and 91 μM at 20 cm for SDRO and SDT3-D, respectively). Porewater NO_2^- (Suppl.

588 Table 1) and NO_3^- (Figs. 2 F-J & F G-L) concentrations were at or near zero below 2 cm at every

589 station, except at SDRO and NDT3-A where large peaks in NO_3^- (376 and 81 μM , respectively)

590 and NO_2^- (37 and 5 μM , respectively) occurred in the top 1 cm.

591

592 Porewater Fe^{2+} concentrations (Figs. 2 F-J & 3 G-L) were several orders of magnitude higher at

593 shallower D stations (max. 722 and 395 μM at NDT3-D and SDT3-D, respectively) compared to

594 depocenter stations (max. 13 and 51 μM at NDRO and SDRO, respectively). NDT3-C porewater

Deleted: showed patterns very similar to total alkalinity,

Deleted: Porewater DIC also increased with basin depth; depocenter sediment had higher DIC concentrations (max. 8.3 mM at NDRO) than D-station (max. 2.8 mM at NDT3-D).

Deleted: PO_4^{3-} concentration increased by approx. one order of magnitude between the core supernatant and the 0-1 cm section at most stations (e.g., 7 and 48 μM at NDRO, respectively). ...

Deleted: NH_4^+ concentration increased by approx. one order of magnitude between the core supernatant and the 0-1 cm section at most stations (e.g., 16 μM and 139 μM at NDRO, respectively). Supernatant NH_4^+ was below detection at D and C stations (and SDT3-B) and above 10 μM at the deeper A (except SDT1-A) and depocenter stations.

Deleted: fig.

Deleted: concentration

Deleted: .

Deleted: NO_3^- concentration decreased substantially in the transition from core supernatant to the 0-1 cm section at most stations (e.g., 24 μM and 0 μM at NDT3-D, respectively). Sediment cores from

Deleted: stations exhibited

Deleted: strong

Deleted:

Moved (insertion) [2]

619 Fe²⁺ concentration (Fig. 2G) peaked in the top 1 cm of sediment (similar to deeper stations)
620 while SDT3-C porewater Fe²⁺ concentration (Fig. 3H) peaked around 5-cm sediment depth. Fe²⁺
621 concentrations reached a max. at 0-2 cm and declined sharply with depth in depocenter and A-
622 station sediment. Northern basin sediment was similar, but the decline in Fe²⁺ below 0-2 cm was
623 less pronounced.

624
625 Maximum porewater sulfide concentrations (Figs. 2 F-J & 3 G-L) were several orders of
626 magnitude lower at the shallower D-stations (5 and 4 μM at NDT3-D and SDT3-D, respectively)
627 compared to A stations (350 and 148 μM at NDT3-A and SDT1-A, respectively). Unlike Fe²⁺,
628 peaks in sulfide concentration occurred deeper in the sediment (e.g., below 5 cm depth at A
629 stations). Porewater sulfate concentrations (Figs. 2 K-O & 3 M-R) decreased slightly with depth,
630 but never reached values below 20 mM at any station.

632 3.4 In-situ microprofiling

633 Microprofiler O₂ and sulfide measurements are shown in Fig. 4. Oxygen was rapidly consumed
634 within the first 0-1 cm of sediment at every station where O₂ was detected in the bottom water
635 (i.e., at all stations except NDRO, which showed no positive signal of oxygen in the water
636 compared to the sediment; note that no oxygen profile is available for SDRO). Sulfide
637 concentrations from microsensors showed similar trends to spectrophotometric measurements,
638 albeit with different absolute values, (below detection in shallower B-, C- and D-stations that
639 lacked mats and >1,000 μM at A- and depocenter stations). Microprofiler pH (Fig. 4) was near
640 7.5 in the bottom water at all stations, and slowly decreased to near 7.0 in the lower parts (3-5

Deleted:

Deleted: , SDRO, and SDT3-A,

Deleted: were anoxic

Deleted: (e.g., 196 and 808 μM sulfide at the 7 cm depth at NDT3-A using the cline method and microprofilers, respectively)...

Deleted: . Sulfide was

Deleted: of the microprofilers

Deleted: (B, C, and D), all of which lacked GSOB mats.

Deleted: The A and depocenter stations had high sulfide concentrations (>...

Deleted:)

Deleted: in the sediment underlying GSOB mats

Deleted: , which rapidly decreased towards zero near the sediment-water interface.

Moved (insertion) [1]

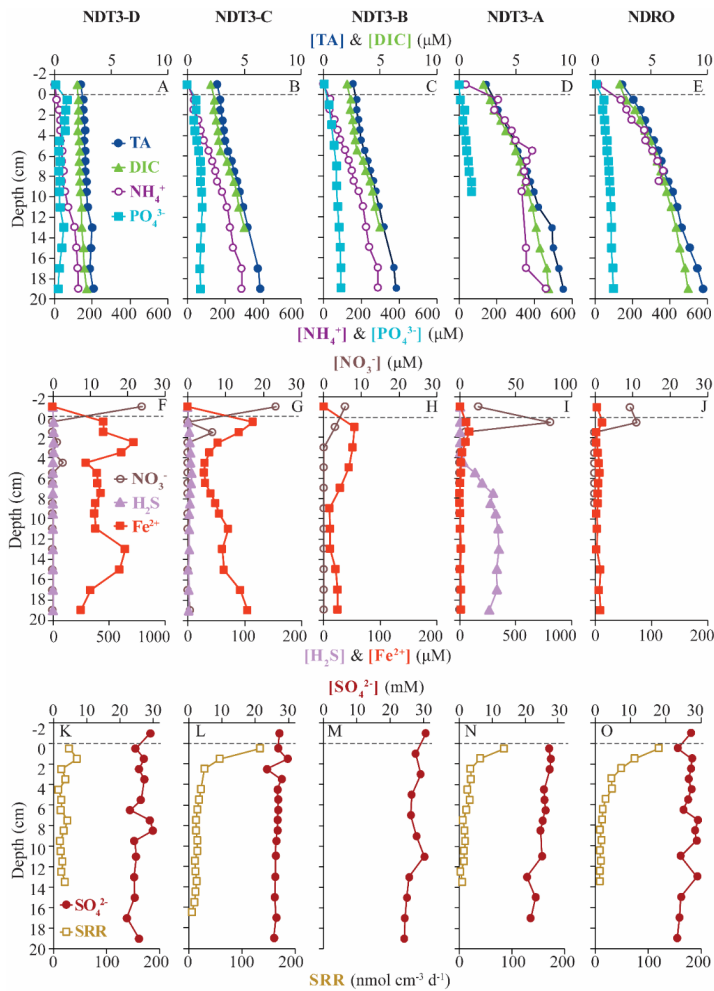
Deleted: with

Deleted: top 20 cm of

Formatted: Not Highlight

658 cm) sediment at most stations except NDT3-C and SDT3-B, pH at 2.5 cm at SDT3-B reached
 659 6.77, which was the lowest observed during this expedition.

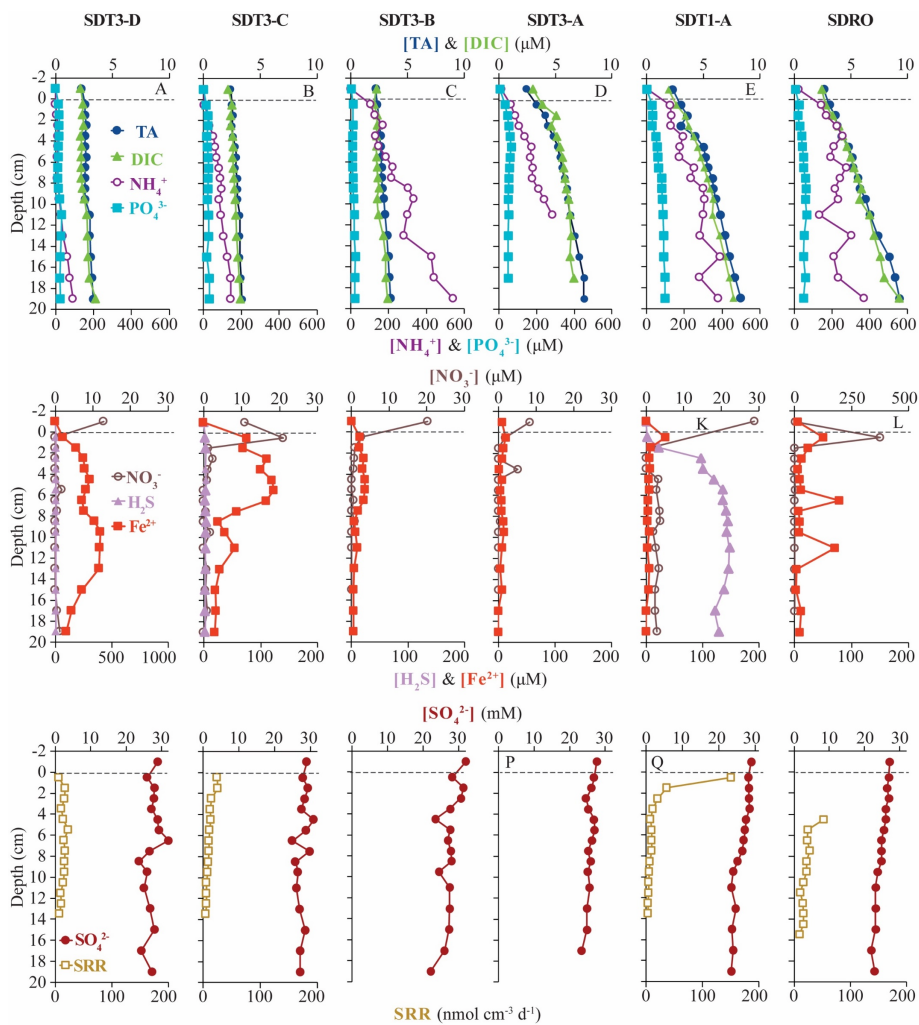
Deleted: all
 Deleted: most stations
 Deleted: 5
 Deleted: At NDT3-C and SDT3-D, pH exhibited no discernible trend over depth with values remaining around pH 7.5. ...



661
 662 **Figure 2.** Biogeochemical data from ROV sediment push cores collected at stations on the northern transect
 663 (NDT3) and in the northern depocenter (NDRO): total alkalinity (TA), dissolved inorganic carbon (DIC),
 664 ammonium (NH_4^+), phosphate (PO_4^{3-}) in the first row; nitrate (NO_3^-), total sulfide (sulfide), and iron (II) (Fe^{2+})
 665 in the second row; sulfate (SO_4^{2-}) and bacterial sulfate reduction rate (SRR) in the third row. Data analyzed from
 666 sediment core supernatant are plotted at -1 cm sediment depth; the dotted line connotes the sediment-water

673 interface. Note the change in scale on the primary x-axis in panel I and the change in scale of the secondary x-
 674 axis in panels F and I. No spectrophotometric sulfide data is available for NDRO and NDT3-B and no SRR data
 675 is available for NDT3-B. For station details see Fig. 1 and Table 1.

Deleted: are

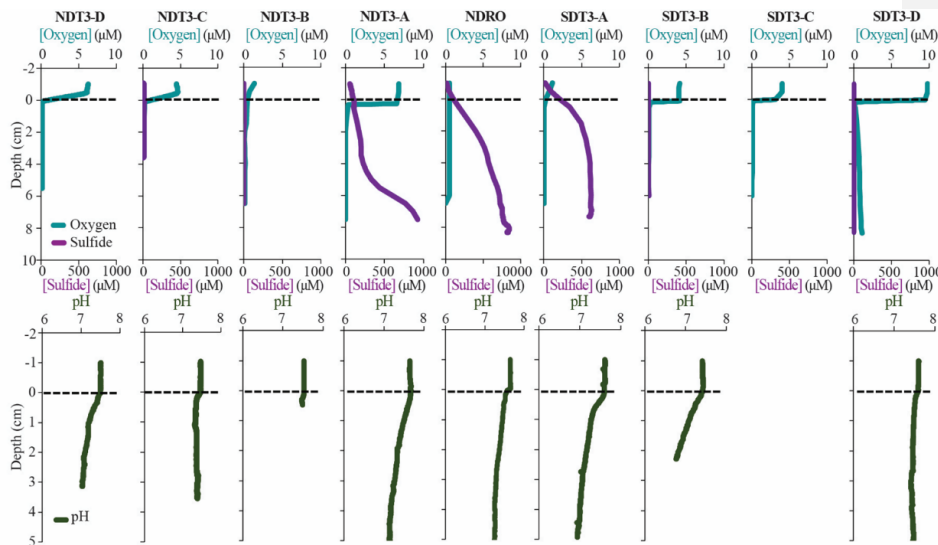


677
 678 **Figure 3.** Biogeochemical data from ROV sediment push cores collected at stations on the two southern
 679 transects (SDT1 and SDT3) and the southern depocenter (SDRO): total alkalinity (TA), dissolved inorganic
 680 carbon (DIC), ammonium (NH_4^+), phosphate (PO_4^{3-}) in the first row; nitrate (NO_3^-), total sulfide (sulfide), and
 681 iron (II) (Fe^{2+}) in the second row; sulfate (SO_4^{2-}) and bacterial sulfate reduction rate (SRR) in the third row. Data
 682 analyzed from sediment core supernatant are plotted at -1 cm sediment depth; the dotted line connotes the

684 sediment-water interface. Note the change in scale on the primary x-axis in panel L and the change in scale of
 685 the secondary x-axis in panel G. No sulfide nor SRR data are available for SDT3-B and -A; spectrophotometric
 686 sulfide data and the top 0-4 cm of SRR data are not available for SDRO. For station details see Fig. 1 and Table
 687 1.
 688

Deleted: at SDRO,

Moved up [1]: To near 7.0 within the top 20 cm of sediment at most stations. At NDT3-C and SDT3-D, pH exhibited no discernable trend over depth with values remaining around pH 7.5.



689
 690
 691 **Figure 4.** In-situ sediment microprofiler results for all stations (except SDT1-A and SDRO): oxygen (O₂) and
 692 total sulfide (sulfide) concentration in the first row; pH profiles in the second row. Note the change in scale on
 693 the secondary x-axis for NDRO sulfide. Values determined in the overlying water are plotted at negative
 694 sediment depths; the dotted line connotes the sediment-water interface.
 695

696 3.5 In-situ fluxes of benthic solutes

697 NO₃⁻, NH₄⁺, PO₄³⁻, and Fe²⁺ flux measured in the BFC revealed different patterns of uptake and
 698 release from the sediment throughout the basin (Fig. 5 and Suppl. Figs. 1-4). BFC O₂
 699 concentrations were compromised by O₂ release from the chamber's polycarbonate walls, which
 700 prevented an accurate calculation of O₂ fluxes from BFC sensor data. NO₃⁻ was consumed at all
 701 stations as indicated by a negative flux (i.e., a flux into the sediment). On the contrary, benthic
 702 release (i.e., a flux out of the sediment) was observed for all other analyzed solutes (NH₄⁺, PO₄³⁻,

708 and Fe^{2+}), with the lowest fluxes in the shallow D and C-stations and highest fluxes in the
 709 depocenter. Ammonium fluxes were the highest of all the determined solutes and showed the
 710 largest difference between deep and shallow stations, with a flux of $1.6 \text{ mmol m}^{-2} \text{ d}^{-1}$ at NDT3-C
 711 (there were no measurable NH_4^+ fluxes in D-station chambers) and reaching $11.1 \pm 3.1 \text{ mmol m}^{-2}$
 712 d^{-1} ($n = 3$) at the two depocenter stations. The depocenter ammonium flux far-outpaced the
 713 concomitant flux of nitrate into depocenter sediments ($-3.2 \pm 0.7 \text{ mmol m}^{-2} \text{ d}^{-1}$, $n = 3$). Iron and
 714 phosphate fluxes were similar at depocenter stations (4.1 ± 0.7 , $n = 3$, and 3.2 ± 0.7 , $n = 3$, mmol
 715 $\text{m}^{-2} \text{ d}^{-1}$, respectively). Alkalinity and DIC concentrations from flux chambers (Suppl. Figs. 5 and
 716 6) remained constant at all stations and thus no DIC flux was calculated. Results from BFCs
 717 injected with $^{15}\text{N-NO}_3^-$ at the SDRO and NDT3-D station are shown in Fig. 6. The rates of
 718 denitrification, anammox, and N_2O production were higher at SDRO compared to NDT3-D.
 719 $^{15}\text{NH}_4^+$ production (DNRA) was one order of magnitude higher at the SDRO station (2.67 mmol
 720 $\text{m}^{-2} \text{ d}^{-1}$) compared to the NDT3-D station ($0.14 \text{ mmol m}^{-2} \text{ d}^{-1}$). DNRA accounted for a much
 721 higher percentage of NO_3^- reduction at SDRO (54.1%) than NDT3-D (13.3%).

722 723 3.6 Sulfate reduction rates

724 Vertical profiles of bacterial sulfate reduction as determined by the radioisotope technique
 725 differed throughout the basin (Figs. 2 & 3). Peaks in sulfate reduction were seen in the top 0-1
 726 cm of sediment at stations with a visible GSOB mat on the surface (120.2, 151.0, and 85.3 nmol
 727 $\text{cm}^{-3} \text{ d}^{-1}$ at NDRO, SDT1-A, and NDT3-A, respectively). Sediments at most shallower basin
 728 depths exhibited peaks slightly deeper in the sediment and of lower magnitude (25.5, 44.5, 22.5
 729 $\text{nmol cm}^{-3} \text{ d}^{-1}$ at SDT3-C, NDT3-D, and SDT3-D respectively). NDT3-C had no visible GSOB
 730 mats but exhibited a peak ($133.7 \text{ nmol cm}^{-3} \text{ d}^{-1}$) in sulfate reduction at 0-1 cm depth, similar to

Deleted: but there was no discernable trend between the two solutes at shallower stations

Deleted:)

Deleted: 4

Deleted: 0

Deleted:

Deleted: (120.2, 151.0, 85.3 $\text{nmol cm}^{-3} \text{ d}^{-1}$)

Deleted: (SDT3-C, NDT3-D, and SDT3-D)

Deleted:

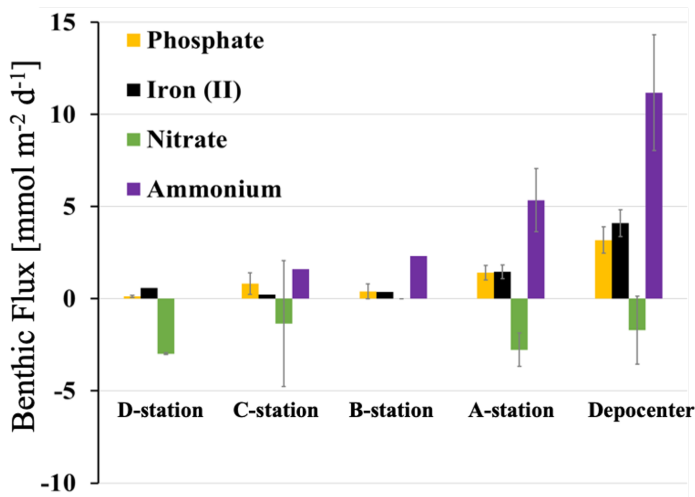
Deleted: present

Deleted: also

Deleted: mirroring

743 deeper stations (e.g., NDRO in Fig. 2O), which differed from other shallow stations (e.g., SDT3-
 744 C in Fig. 3N). The integrated sulfate reduction rate (0-14 cm depth) at NDRO ($4.1 \text{ mmol m}^{-2} \text{ d}^{-1}$)
 745 was noticeably higher than most other stations with the exception of NDT3-C ($3.8 \text{ mmol m}^{-2} \text{ d}^{-1}$)
 746 (Table 2). NDT3-D and NDT3-C exhibited higher integrated rates (2.9 and $3.8 \text{ mmol m}^{-2} \text{ d}^{-1}$)
 747 than their southern station counterparts SDT3-D and SDT3-C (1.9 and $1.7 \text{ mmol m}^{-2} \text{ d}^{-1}$).
 748

- Moved (insertion) [4]
- Deleted: deeper sulfate reduction profiles
- Deleted: .the sulfate reduction rate at NDT3-C (Fig. 2L) mirrored deeper station profiles
- Deleted: rather than
- Deleted: profiles
- Moved (insertion) [5]
- Deleted: I
- Deleted:
- Deleted: ¶



749
 750
 751 **Figure 5.** Benthic fluxes of solutes (positive flux = release from the seafloor; negative flux = uptake by the
 752 seafloor) determined with in-situ benthic flux chambers. Rates were averaged for stations of same depth from
 753 the northern and southern transect and the depocenter (NDRO and SDRO). Note, giant sulfur-oxidizing bacterial
 754 mats were found at depocenter and A-stations. Error bars represent standard errors.
 755

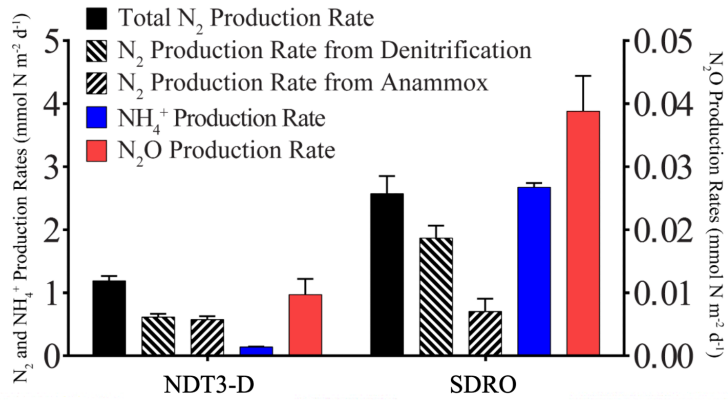


Figure 6. Areal rates of total N₂ production, denitrification, anammox, NH₄⁺ production (DNRA), and N₂O production

773
774
775
776
777

778

Moved up [5]: Integrated sulfate reduction rate (0-14 cm depth) at NDRO (4.1 mmol m⁻² d⁻¹) was noticeably higher than most other stations with the exception of NDT3-C (3.8 mmol m⁻² d⁻¹) (Table 2). NDT3-D and NDT3-C exhibited higher integrated rates (2.9 and 3.8 mmol m⁻² d⁻¹) than their southern station counterparts SDT3-D and SDT3-C (1.9 and 1.7 mmol m⁻² d⁻¹).

Deleted: Sulfate reduction rates at depocenter and A stations decreased sharply below 0-1 cm sediment depth (up to an order of magnitude decrease at NDRO and SDT1-A), while remaining low and steady over depth in C and D station sediment. ...

791 **4. Discussion**

792 **4.1 Giant sulfur-oxidizing bacterial mats proliferated in response to deoxygenation in the**

793 **Santa Barbara Basin**

794 The SBB is an ideal environment to study the effect of transient deoxygenation on benthic

795 biogeochemistry. In ~~Fall 2019, when this expedition took place,~~ the SBB was undergoing a

Deleted: November

796 transition from oxygenated to ~~virtually~~ anoxic conditions (Qin et al., 2022). When the AT42-19

797 cruise occurred, most of the bottom water in the basin was hypoxic (~~A-, B-, C-, and D-~~stations),

Deleted:

798 except for the depositional center. ~~Separate O₂ measurements from the ROV sensor (O₂ below~~

Deleted: Importantly, s

799 ~~detection limit,~~ Table 1), microprofilers (~~no signal change between water column and sediment,~~

800 Fig. 4), and Winkler titration from CTD/rosette casts (~~uniform non-zero value below 500 m~~ (Qin

801 et al., 2022)) indicated full anoxia in the bottom water at the deeper stations (~~NDRO and SDRO~~).

Deleted: se

802 Notably, bottom water conditions revealed a slight asymmetry between the basin transects (Fig.

803 1); bottom water along the northern transect generally ~~had~~ more O₂ and NO₃⁻ than the southern

Deleted: had

804 transect (e.g., 9 μM O₂ at NDT3-A and 0 μM O₂ at SDT3-A). This asymmetry indicated

805 differences in the circulation and/or microbial communities between the northern and southern

806 portions of the basin. Whether this asymmetry is a permanent feature of the basin or

807 symptomatic of the specific conditions in November 2019 is unclear; previous studies in the SBB

808 have been restricted to the depocenter or one side of the basin (Sholkovitz, 1973; Reimers et al.,

809 1996a; Kuwabara et al., 1999). Regardless of bottom water oxidant concentration, the

810 energetically most ~~favorable~~ terminal electron acceptors (O₂ and NO₃⁻) disappeared in a very

Deleted: powerful

811 narrow zone below the sediment-water interface (Fig. 4 and Figs. 2 and 3, respectively),

812 consistent with their expected rapid consumption by the benthic microbial community.

813

820 In the present study, benthic GSOB mats were primarily limited to the anoxic depocenter of the
821 SBB. Similarly, such mats were replete in the core of the anoxic Peruvian OMZ (Levin et al.,
822 2002; Sommer et al., 2016; Mosch et al., 2012), but absent from the seafloor below the hypoxic,
823 i.e., slightly oxygenated, Mauritanian OMZ (Schroller-Lomnitz et al., 2019). GSOB mats in
824 November 2019 were observed deeper in the basin than in October 2013 (Valentine et al., 2016)
825 but in a similar location to June 1988 (Reimers et al., 1996a) and April 1997 (Kuwabara et al.,
826 1999). During the 2013 sampling, dense GSOB mats were confined to depths between approx.
827 500-570 m (equivalent to the B₂ stations from this expedition), corresponding with anoxic
828 conditions in the bottom water. This habitat was sandwiched between an anoxic, anitric (i.e.,
829 nitrate-free) deep and a hypoxic, nitrogenated (i.e., nitrate-rich) shallower water layer (Valentine
830 et al., 2016). The difference in depth distribution of GSOB mats between the 2013 and 2019
831 expedition provides evidence that GSOB mats in the SBB are ephemeral and proliferate where
832 the bottom water is anoxic but not anitric.
833
834 As our study represents only a snapshot of an oxygen- and nitrate-driven mat dynamic, we can
835 only speculate how areas of the basin that did not contain GSOB mats in November 2019 fit into
836 this dynamic. For example, mat-forming sulfur bacteria found slightly deeper in the sediment at
837 B₂ stations (see section 3.2) could be progenitors to surface sediment colonization of thick GSOB
838 mats, as has been recorded in other transiently deoxygenated environments (Jørgensen, 1977).
839 Alternatively, these subsurface colonies could also be remnants of a former surface GSOB mat
840 that retreated under changing redox conditions. Oxygenated conditions in the water preceding
841 the 2019 expedition would, in this context, suggest the mats migrated following a previous
842 anoxic event (Qin et al., 2022). If deoxygenation persisted in the SBB after the AT42-19 cruise,

Deleted: The sediment-water interface represents the front-line in a battle between microbes for powerful electron acceptors. ...

Deleted: supposedly

Deleted:

Deleted:

Deleted:

Deleted: it

Deleted: mean

852 then anitria (i.e., anitric conditions - similar to anoxia) would likely follow in the deepest basin
 853 water. These conditions would be similar to those seen ~~in 2013~~ (Valentine et al., 2016), where
 854 GSOB mats formed a contiguous “donut ring” at shallower basin depths. ~~Interestingly, GSOB~~
 855 ~~mats in the Eastern Gotland Basin of the Baltic Sea were confined to a hypoxic transition zone,~~
 856 ~~where O₂ was < 30 μM but did not reach anoxia, while no mats were observed at deeper anoxic~~
 857 ~~locations~~ (Noffke et al., 2016). ~~This difference in distribution compared to the SBB suggests that~~
 858 ~~GSOB mats proliferate under different conditions (anoxic or hypoxic), potentially depending on~~
 859 ~~the species of mat-forming bacteria present and whether they specialize in aerobic or anaerobic~~
 860 ~~chemosynthesis.~~

- Deleted: during
- Deleted: the
- Deleted: expedition by D. Valentine and co-workers
- Deleted: the

862 **4.2 Shift from benthic denitrification to dissimilatory nitrate reduction to ammonium in**
 863 **response to complete deoxygenation in the Santa Barbara Basin**

865 Benthic ~~uptake and release~~ of nitrogen species by SBB sediment appeared to be affected by the
 866 presence of GSOB mats. While ~~total~~ benthic nitrate ~~uptake was similar between D- and~~
 867 ~~depo-center stations,~~ based on ~~in-situ NO₃⁻ flux measurements (Fig. 4),~~ NH₄⁺ release from the
 868 sediment into the water column increased ~~where GSOB mats were present~~ (Fig. 5). This trend is
 869 supported by the porewater profiles of NH₄⁺, which ~~showed a steeper increase over sediment~~
 870 ~~depth at deeper stations,~~ (Figs. 2 & 3). Incubations with ¹⁵N-NO₃⁻ revealed that N₂ production
 871 ~~(denitrification and anammox) accounted for 86% of NO₃⁻/NO₂⁻ reduction in the shallow basin,~~
 872 ~~while NH₄⁺ production (DNRA) accounted for 13% and N₂O production accounted for 1%~~
 873 ~~(NDT3-D, Fig. 6; (Peng et al., 2023)). In contrast, most (54%) of NO₃⁻ reduction at the~~
 874 depositional center occurred via DNRA; ~~N₂ production accounted for 45% and N₂O production~~

- Deleted: release and
- Deleted: consumption
- Deleted: not significantly different
- Deleted: was unaffected by GSOB mats
- Deleted: remained unchanged
- Deleted: evident at all stations
- Deleted: porewater and
- Deleted: with station depth
- Deleted: faster
- Deleted: with
- Deleted: tend to increase in steepness with
- Deleted: depth
- Deleted: via
- Deleted: removal
- Deleted:
- Deleted: Conversely
- Deleted: 54%
- Deleted: removal
- Deleted: ,

898 accounted for 1% of NO₃⁻ reduction at the SDRO (Fig. 6; Peng et al. 2023). It is important to
899 note that these results only describe patterns of NO₃⁻ reduction in the basin, while other
900 mechanisms of nitrate uptake by sediment (e.g., hyper-accumulation of nitrate into vacuoles) are
901 more difficult to calculate accurately. It is also important to note that diatoms hyper-accumulate
902 nitrate (Kamp et al., 2011) and meiofauna (e.g., nematodes) can positively impact rates of
903 denitrification (Bonaglia et al., 2014). Both diatoms and meiofauna were seen in SBB depocenter
904 and A-station sediments in November 2019 (data not shown), so their impact on SBB benthic
905 nitrogen cycling is likely important and remains to be disentangled from the mats themselves.

906
907 This data suggests a transition from denitrification-dominated sediment in the oxygenated basin
908 to an increasing influence of DNRA on N₂ cycling in the deeper, anoxic basin. Placed in the
909 context of other OMZs, Mauritanian shelf sediment was dominated by denitrification (Dale et al.,
910 2014), similar to SBB shallow sediment (below hypoxic water) while core Peruvian OMZ
911 sediment was dominated by DNRA, similar to sediment of the deeper SBB (below anoxic water),
912 (Sommer et al., 2016). Nitrate reduction in sediment below the seasonally hypoxic Eckernförde
913 Bay (Dale et al., 2011) and below the hypoxic transition zone of the Eastern Gotland Basin
914 (Noffke et al., 2016) also showed increased DNRA where GSOB mats were present, though with
915 an order of magnitude lower NH₄⁺ flux (avg. 1.74 mmol m⁻² d⁻¹ and max. 1.10 mmol m⁻² d⁻¹
916 respectively) than the SBB depocenter.

917
918 While our study suggests a shift from denitrification to DNRA during deoxygenation of SBB
919 bottom water, other studies examined changes in benthic nitrogen cycling under reverse
920 conditions, i.e., the reoxidation of the environment following anoxia (Hylén et al., 2022; De

Deleted: (

Deleted: ,

Deleted: s

Deleted: -

Deleted: nitrate reduction in the shallow SBB sediment (below hypoxic water) was similar to

Deleted: nitrate reduction in the

Deleted: was similar to the core Peruvian OMZ

Deleted:

930 Brabandere et al., 2015). After a decadal oxygenation event in the Eastern Gotland Basin (Baltic
 931 Sea) in 2015-2016, sediment exhibited a slight increase in denitrification, but remained
 932 dominated by DNRA and N₂O production (Hylén et al., 2022). The lack of N₂ production via
 933 denitrification following this oxygenation event was attributed to the reoxygenation event being
 934 too weak to substantially oxidize sediments, which would favor denitrification (Hylén et al.,
 935 2022). In an engineered reoxygenation event of the By Fjord on Sweden's western coast, where
 936 dissolved O₂ and NO₃⁻ content of anoxic and anoxic bottom water was artificially increased to
 937 approx. 130 μM O₂ and 20 μM NO₃⁻ over a period of roughly 2 years, denitrification rates were
 938 increased by an order of magnitude and DNRA rates were also stimulated (De Brabandere et al.,
 939 2015). Comparing our results to these two studies suggests that DNRA bacteria are more
 940 resilient to weak reoxygenation events and thrive in transiently deoxygenated systems that
 941 remain hypoxic (O₂ < 63 μM). The frequency and magnitude of reoxygenation and
 942 deoxygenation of SBB bottom waters, and the effect of these processes on the benthic microbial
 943 community, could be a major factor supporting some of the highest recorded total nitrate
 944 reduction rates in a natural benthic marine setting (Peng et al., 2023).

Deleted: s

Deleted: ti

Deleted: approx.

Deleted: approx.

Deleted: in why

945 **Table 3.** Example reactions of nitrate reduction pathways with associated energy yield in respect to the electron
 946 donor (H₂ or HS⁻) and electron acceptor (NO₃⁻) and electron accepting capacity. Modified from Table 2 in (Tiedje
 947 et al., 1983).

Reaction	ΔG° (kcal mol ⁻¹)		Electrons per NO ₃ ⁻
	H ₂ / HS ⁻	NO ₃ ⁻	
Chemoheterotrophic Denitrification			
2NO ₃ ⁻ + 5H ₂ + 2H ⁺ → N ₂ + 6H ₂ O	-53.6	-133.9	5
Chemoautotrophic Denitrification			
8NO ₃ ⁻ + 5HS ⁻ + 3H ⁺ → 5SO ₄ ²⁻ + 4N ₂ + 4H ₂ O	-177.9	-111.2	5
Chemoheterotrophic DNRA			
NO ₃ ⁻ + 4H ₂ + 2H ⁺ → NH ₄ ⁺ + 3H ₂ O	-35.8	-143.3	8
Chemoautotrophic DNRA			
NO ₃ ⁻ + HS ⁻ + H ⁺ + H ₂ O → NH ₄ ⁺ + SO ₄ ²⁻	-107.0	-107.0	8

948

949

955 A high ratio of electron donor to electron acceptor favors DNRA over denitrification, (Marchant
956 et al., 2014; Hardison et al., 2015; Tiedje et al., 1983) and this ratio appears to be critical in
957 determining the dominant nitrate reduction pathway in SBB sediments, similar to the Eastern
958 Gotland Basin (Hylén et al., 2022) and the By Fjord (De Brabandere et al., 2015). Example
959 energy yields for denitrification and DNRA are shown in Table 3. As discussed in (Tiedje et al.,
960 1983), heterotrophic denitrification yields more energy per mol of electron donor than DNRA.
961 However, the reverse is true when considering energy yield per mol of electron acceptor (NO₃⁻).
962 DNRA also yields 3 more electrons per molecule of NO₃⁻ than denitrification. Tiedje et al.
963 argued that in environments that are starved of powerful terminal electron acceptors, such as
964 anoxic, organic-rich sediment, the energy yield per electron acceptor and additional electrons
965 available for transfer could push nitrate reduction towards DNRA. Multiple laboratory and
966 model studies have converged on an electron donor to acceptor ratio of approximately 3 to
967 encourage DNRA over denitrification (Hardison et al., 2015; Algar and Vallino, 2014) though
968 other studies have found higher values (Porubsky et al., 2009; Kraft et al., 2014). Sulfide
969 concentrations near the sediment-water interface at the SBB depocenter (approx. 200 μM at 0.5
970 cm depth; Fig. 3, NDRO) would favor chemoautotrophic DNRA over denitrification at ambient
971 marine nitrate concentrations (approx. 28 μM). Additionally, DNRA appears to be the preferred
972 nitrate reduction pathway for chemoautotrophs that utilize iron or sulfide as an electron donor
973 (Caffrey et al., 2019; Kessler et al., 2019; An and Gardner, 2002). As GSOB mats hyper-
974 accumulate nitrate from the bottom water into their intracellular vacuoles, the resulting decline in
975 electron acceptors at the sediment-water interface coupled with an elevation of the sulfate
976 reduction zone would create an electron donor to acceptor ratio that favors DNRA. Since GSOB
977 mats in the SBB seem to prefer DNRA, starving the bottom water of electron acceptors coupled

Moved (insertion) [8]

Field Code Changed

Deleted: .

Deleted: A

980 with the high sulfate reduction rates could give them a competitive advantage and allow them to
 981 proliferate into the largest-yet mapped GSOB mat in Earth's oceans, as seen in other expeditions
 982 (Valentine et al., 2016; Reimers et al., 1996a; Kuwabara et al., 1999).

983

984 **4.3 Microbial mat proliferation and benthic phosphate remineralization dependent on high**
 985 **rates of organic matter degradation in the Santa Barbara Basin**

986

987 Organic carbon content of the benthic environment appears to be a key control on sulfate
 988 reduction rates near the sediment-water interface as well as microbial mat proliferation. Sulfate
 989 reduction rates in the SBB depocenter are most similar in magnitude and profile (i.e., highest
 990 rates found at the sediment-water interface and decline drastically thereafter) to those found in
 991 sediments below the transiently deoxygenated portion of the Peruvian shelf (e.g., 4.1 mmol m⁻²
 992 d⁻¹ at the SBB NDRO station vs. 2.5-3.8 mmol m⁻² d⁻¹ at 128-144 m water depth on the Peruvian
 993 margin (Gier et al., 2016; Treude et al., 2021)). The TOC content of surface sediments in these
 994 two regions are both high and within the same order of magnitude (maximum recorded TOC of
 995 5.2% at the 0-1 cm margin at the SDT1-A station compared with 7.6% in the Peruvian margin
 996 145 m depth (Noffke et al., 2012)). In comparison, sulfate reduction rates in the SBB were at
 997 least one order of magnitude lower than found in sediment below the OMZ on the Namibian
 998 Shelf, which has much higher TOC contents of >10% (Brüchert et al., 2003; Bremner, 1981).
 999 Sulfate reduction rates in the shelf sediments below the Eastern Arabian OMZ were much lower
 1000 (0.18 – 1.27 mmol m⁻² d⁻¹) than rates in the SBB depocenter (Naik et al., 2017) despite similar
 1001 hypoxic to anoxic bottom water conditions. These lower sulfate reduction rates were attributed to
 1002 the relatively low amount of pelagic primary productivity and ergo benthic organic matter

Moved up [8]: (Marchant et al., 2014; Hardison et al., 2015; Caffrey et al., 2019; Kessler et al., 2019; An and Gardner, 2002).

Moved up [6]: Anoxia could trigger the uptake of NO₃⁻ into vacuoles, creating declining NO₃⁻ concentrations that are more favorable to DNRA in the bottom water. In these conditions, GSOB in the SBB benthic environment could utilize their ability to perform DNRA to out-compete similar denitrifying taxa, and proliferate into thick, contiguous mats. While low-nitrate conditions could benefit GSOB mats, the mats do not persist once bottom water reaches anoxia, as evidenced by GSOB mat distribution during the 2013 expedition (Valentine et al., 2016).¶

Moved (insertion) [6]

Deleted: →¶
 Declining nitrate concentrations may be as important as anoxia itself to GSOB mat proliferation. Anoxia could trigger the uptake of NO₃⁻ into bacterial vacuoles, creating declining NO₃⁻ concentrations that are more favorable to DNRA in the bottom water. In these conditions, GSOB in the SBB benthic environment could utilize their ability to perform DNRA to out-compete similar denitrifying taxa, and proliferate into thick, contiguous mats. High ratios of electron donor (organic matter or sulfide) to electron acceptor (nitrate) encourage DNRA over denitrification (Marchant et al., 2014; Hardison et al., 2015; Caffrey et al., 2019; Kessler et al., 2019; An and Gardner, 2002). In these nitrate-deficient areas in the ocean, DNRA linked to anaerobic ammonium oxidation (anammox) can be more thermodynamically favorable and thus organisms that participate in this consortium could have a competitive advantage over other denitrifying organisms (Jensen et al., 2011). NO₂⁻ was at or near-zero concentrations in the sediment porewater of all stations, except in the 0-1 cm depth interval of two stations (SDRO and NDT3-A) featuring GSOB mats (Suppl. Table 1). These spikes in NO₂⁻ (an... [1])

Deleted: (Marchant et al., 2014; Hardison et al., 2015; Caffrey et al., 2019; Kessler et al., 2019; An and Gardner, 2002). In these nitrate-deficient areas in the ocean, DNRA linked to anaerobic ammonium oxidation (anammox) can be more thermodynamically favorable and thus organisms (... [2])

Deleted: . In these nitrate-deficient areas in the ocean, DNRA linked to anaerobic ammonium oxidation (anammox) can be more thermodynamically favorable and thus organisms that participate in this consortium could have a competitive advantage over other denitrifying organisms (Jensen et al. (... [3])

Deleted: (Reimers et al., 1996a). GSOB mats can be associated with symbiotic anaerobic ammonium-oxidizing (anammox) bacteria (Prokopenko et al., 2006). Since the anammox process utilizes NO₂⁻ as the electron acceptor and NH₄⁺ as the electron donor, a consortium of GSOB mat (... [4])

Deleted: . GSOB mats can be associated with symbiotic anaerobic ammonium-oxidizing (anammox) bacteria (Prokopenko et al., 2006). Since the anammox process utilizes NO₂⁻ as the electron acceptor and NH₄⁺ as the electron donor, a consortium of GSOB mats and anammox bacteria wer (... [5])

Deleted: delivery to

Deleted: .

1186 delivery in the Eastern Arabian OMZ compared to other upwelling systems (Naik et al., 2017).
1187 The organic matter content of the sediment appears to be important in the proliferation of GSOB
1188 mats; too much TOC could result in toxic levels of sulfide at the sediment-water interface
1189 (*Beggiatoa* exhibit an aversion to sulfidic sediments but toxicity has not been quantified)
1190 (Preisler et al., 2007), whereas too little sulfide would not provide enough electron donor for the
1191 GSOB's chemoautotrophic metabolism.

Deleted: transiently deoxygenated

1192
1193 The profiles of several indicators for benthic anaerobic organic matter remineralization (total
1194 alkalinity, DIC, PO_4^{3-} , NH_4^+) increased in steepness with increasing water depth (Figs. 2 A-E &
1195 3A-F). One divergence from this trend can be seen in PO_4^{3-} profiles from the shallow C₂ and D₂
1196 stations, which also featured low rates of sulfate reduction. PO_4^{3-} profiles in these sediments
1197 track closely to Fe^{2+} profiles; both solutes dip in concentration in areas with visible iron sulfide
1198 formation (e.g., 5-11 cm in NDT3-D as seen in Fig. 2A). Additionally, several stations that
1199 exhibited high sulfate reduction rates in surface sediment (e.g., SDT1-A) showed almost no
1200 change in PO_4^{3-} at depths below 5 cm (e.g., Fig. 2 K-O compared to Fig. 2 A-E). This
1201 phenomenon has been previously documented in SBB sediment and is attributed to the
1202 precipitation of carbonate fluorapatite (Reimers et al., 1996a). The confinement of these flat
1203 PO_4^{3-} profiles to stations with $>100 \text{ nmol cm}^{-3} \text{ d}^{-1}$ sulfate reduction in surface sediment suggests
1204 that this mineralogical sink of PO_4^{3-} in SBB sediment may be dependent on high sulfate
1205 reduction rates, owing to the bicarbonate produced by sulfate reduction (Reimers et al., 1996a),
1206 and is not found throughout the basin. Flat PO_4^{3-} profiles were also reported from the transiently
1207 deoxygenated portion of the Peruvian OMZ, where phosphate mineral precipitation has been
1208 documented (Noffke et al., 2012). Similar to the shallow margins of the SBB, PO_4^{3-} in

Deleted:

1211 Mauritanian OMZ porewater tracks closely with changes in porewater Fe²⁺ (Schroller-Lomnitz
1212 et al., 2019), indicating that iron mineralization/dissolution mechanisms hold a greater influence
1213 on PO₄³⁻ concentrations under hypoxic bottom waters.

Deleted: c

1215 **4.4 Iron oxide exhaustion is critical for raising the sulfate reduction zone close to the**
1216 **sediment-water interface in Santa Barbara Basin sediment.**

Deleted: 3

1218 ~~The hyper-accumulation of NO₃⁻ by GSOB mats potentially facilitates sulfate reduction close to~~
1219 ~~the sediment-water interface in the SBB (e.g., NDRO and NDT3-A as seen in fig. 2N and 2O) by~~
1220 ~~starving the sediment of this more powerful electron acceptor. The rise of the sulfate reduction~~
1221 ~~zone at NDT3-C (fig. 2L) further suggests that the exhaustion of iron oxides and the formation of~~
1222 ~~iron sulfide below the sediment-water interface may play a crucial role in controlling the~~
1223 ~~distribution of sulfate reduction as well. SBB sediments showed a wide vertical and horizontal~~

Deleted: While

Deleted: appeared to

Deleted: possibly

Deleted: environment

Deleted: s

Deleted: elevation

Deleted: formation

Deleted: in deeper sediment layers

Deleted: also

1224 heterogeneity of redox states based on visual appearance (Fig. 1A-K). Sediment beneath the
1225 hypoxic bottom water at the shallowest D₂ stations was reddish, consistent with a high content of
1226 iron oxides. Interestingly, porewater Fe²⁺ concentrations in shallower parts of the basin (e.g.,
1227 NDT3-D, max. ~700 μM Fe²⁺) were an order of magnitude larger than those found in both the
1228 Peruvian (max ~60 and ~30 μM Fe²⁺, respectively; (Noffke et al., 2012; Plass et al., 2020) and
1229 Mauritanian (max. ~50 μM Fe²⁺; Schroller-Lomnitz et al 2019) OMZ. ~~It should be noted that~~

Deleted:

Deleted: anywhere

Deleted: It is worth noting

Deleted:

Deleted: as the geochemistry

Deleted: ; the measured

Deleted: which should be considered when comparing to other studies...

Deleted: This is of particular importance for Fe²⁺, h

1230 ~~porewater samples for geochemical analyses were unfiltered and hence reported iron~~
1231 ~~concentrations include aqueous, colloidal, and nanoparticulate species. Regardless, all these~~
1232 ~~components represent bioavailable sources of iron. Further, since filtering through 0.45 or 0.2~~
1233 ~~μm filters only removes a fraction of colloidal particles and no nanoparticles (Raiswell and~~

Deleted: Irrespective

Deleted: owever

Deleted: all of

Deleted: S

Deleted: with

Deleted: a

Deleted: (

Deleted:)

1262 Canfield, 2012), potential surplus porewater iron in SBB samples in comparison to studies that
 1263 applied filtering was likely minimal.
 1264
 1265 Deeper in the basin, bands of black sediment that appear mid-core at NDT3-C (6-14 cm) and
 1266 SDT3-C (6-10 cm) indicate the formation of iron sulfides as a result of sulfide produced by
 1267 sulfate reduction (Canfield, 1989). Both D-stations had similar bottom water conditions (Table
 1268 1), sulfate reduction rates (Fig. 3W-AG), porewater concentrations of solutes (Figs. 2 and 3), and
 1269 visual sediment characteristics (Section 3.1). On the contrary, there are some noticeable
 1270 differences in the porewater geochemistry between the two C-stations. At the C-stations, peaks
 1271 in sulfate reduction were, in the surface sediment, above the iron sulfide layers, and declined
 1272 below approximately 4 cm, indicating a discrepancy between observed peak sulfate reduction
 1273 activity and the mineralogical clues left behind by the process. Comparing NDT3-C and SDT3-
 1274 C, iron sulfide formation (Table 1B compared to 1J), porewater Fe²⁺ profiles (Fig. 2G compared
 1275 to Fig. 3H), and sulfate reduction rates (Fig. 2L compared to Fig. 3N) show that NDT3-C
 1276 sediment appears to be in transition towards a more sulfidic state, while SDT3-C sediments still
 1277 mimic the shallow D-station ferruginous state. While sulfate reduction rates for B-stations are
 1278 not available due to technical issues during sample processing, porewater Fe²⁺ profiles show a
 1279 similar difference between the north and south basin (Fig. 2H compared to Fig. 3I) as did visual
 1280 sediment characteristics (Table 1C compared to 1I). This difference in biogeochemical profiles
 1281 and apparent mineralogy between the north and south C- and B-stations could be a result of
 1282 hydrographic and/or bathymetric differences in the basin (Sholkovitz and Gieskes, 1971; Bograd
 1283 et al., 2002), but a discernable link between the differences in sediment biogeochemistry and the
 1284 differences in bottom water oxygen (Table 1) need to be further explored.

Deleted: located

Deleted: .

Deleted: Comparing data from shallow stations at with the same depth (e.g., NDT3-C vs. SDT3-C) revealed differences in sediment sulfate reduction in the SBB, potentially due to changes in iron mineralogy. Both D-stations had similar bottom water conditions (Table 1), sulfate reduction rates (Fig. 3W-AG), porewater concentrations of solutes (Figs. 2 and 3), and visual sediment characteristics (Section 3.1). On the contrary, there are some noticeable differences in the porewater geochemistry between the two C-stations, which in contrast to D-stations are below the SBB sill depth, irrespective of similar bottom water oxygen conditions

Deleted: .

Moved up [2]: NDT3-C porewater Fe²⁺ concentration (Fig. 2G) peaked in the top 1 cm of sediment (similar to deeper stations) while SDT3-C porewater Fe²⁺ concentration (Fig. 3H) peaked around 5-cm sediment depth.

Moved up [3]: NDT3-C sediment (Table 1B) exhibited iron sulfide formation from approx. 6-14 cm sediment depth, while SDT3-C sediment (Table 1J) had a much narrower band around 8-10 cm (the same depth at which Fe²⁺ concentrations decrease in the porewater).

Moved up [4]: the sulfate reduction rate at NDT3-C (Fig. 2L) mirrored deeper station profiles (e.g., NDRO in Fig. 2O) rather than other shallow station profiles (e.g., SDT3-C in Fig. 3N). While sulfate reduction rates for B-

Deleted: Finally,

Deleted:

1314

1315 Deeper in the basin (depocenter and A-stations), porewater Fe^{2+} concentrations in sediment
1316 beneath anoxic bottom water (max. $84 \mu\text{M Fe}^{2+}$) were similar to concentrations found below the
1317 Peruvian OMZ in 2008 under anoxic bottom water conditions (78 m water depth, max. $80 \mu\text{M}$
1318 Fe^{2+}) (Noffke et al., 2012). ~~These deep basin~~ porewater Fe^{2+} concentrations were, ~~however,~~ an
1319 order of magnitude larger than those found at a similar site on the Peruvian shelf (75 m water
1320 depth, max. $1 \mu\text{M Fe}^{2+}$) in 2017 during a kelvin-wave-associated “Coastal El Niño” event that
1321 created oxygenated bottom waters during the sampling and the disappearance of previously
1322 observed dense GSOB mats (Plass et al., 2020). As the SBB water column was undergoing rapid
1323 deoxygenation in the weeks preceding this study (Qin et al., 2022), the sediments below the sill
1324 appeared to be actively shifting from a ferruginous state to a sulfidic state, with this change
1325 starting around the C-stations and being complete in the depocenter. Comparing apparent iron
1326 sulfide formation with dips in porewater Fe^{2+} concentrations in C-station profiles (Fig. 1B
1327 compared to Fig. 2G and Fig. 1J compared to Fig. 3H) signals a shift away from a ferruginous
1328 state occurring just below the SBB sill.

1329

1330 C-station porewater Fe^{2+} concentrations and sulfate reduction rates indicate that migration of the
1331 sulfate reduction zone towards the sediment-water interface is associated with iron sulfide
1332 formation deeper in the sediment. The activity ~~(or lack thereof)~~ of cable bacteria, which are able
1333 to bridge the gap between the oxidized sediment-water interface and reduced sediment below
1334 using a biofilament (Pfeffer et al., 2012), could explain the interplay between sulfate reduction
1335 and iron cycling in SBB sediments. Cable bacteria, ~~such as *Ca. Electronema sp.*~~, contain ~~v~~ genes
1336 ~~involved in~~ DNRA (Kjeldsen et al., 2019) and can perform nitrate reduction in incubation

Deleted: SBB

Deleted:

Deleted: the

Deleted: required for

1341 experiments (Marzocchi et al., 2014), but their direct transformation of NO_3^- in the environment
1342 appears limited (Kessler et al., 2019) and they appear to be inactive in anoxic aquatic
1343 environments (Seitaj et al., 2015; Marzocchi et al., 2018; Hermans et al., 2019). Cable bacteria
1344 primarily conduct aerobic sulfide oxidation (Pfeffer et al., 2012), though they can also utilize
1345 Fe^{2+} as an electron donor (Seitaj et al., 2015). The maximum recorded filament length of cable
1346 bacteria is 7 cm (Van De Velde et al., 2016), though typically they are not stretched completely
1347 vertically through the sediment. The appearance of black sediment in the SBB C-station
1348 sediments, starting at approx. 5 cm depth, could be an indication that cable bacteria are oxidizing
1349 iron sulfides at that sediment depth and prevent their formation at shallower depths. Further,
1350 cable bacteria have been found to directly compete with GSOB in transiently deoxygenated
1351 systems, with cable bacteria active under oxygenated conditions and GSOB active in anoxic
1352 conditions (Seitaj et al., 2015). Cable bacteria can also prevent the benthic release of sulfide,
1353 which is toxic to many pelagic animals, via the creation of an iron-oxide buffer (formed through
1354 Fe^{2+} oxidation) in near-surface sediments (Seitaj et al., 2015). Therefore, if cable bacteria activity
1355 in the SBB decreased with declining oxygen concentrations below the sill, the iron oxide buffer
1356 they create could have been reduced, encouraging the sulfate reduction zone to migrate towards
1357 the sediment surface (as seen at NDT3-C). Cable bacteria can sometimes be detected in
1358 sediments via a slight pH increase (typically $\text{pH} > 8$) (Schauer et al., 2014), which was not
1359 reflected in our pH results, but this phenomenon is more typically seen in the laboratory and not
1360 the field (Hermans et al., 2019).

1362 4.5 Iron and phosphate flux into SBB bottom water is a feature of transient deoxygenation.

1363

Deleted: ,

Deleted: roughly in line with the

Deleted: could be

Deleted: organisms

Deleted: ir

Deleted: The presence of c

Deleted: by

Deleted: increase in pH

Deleted: below the sediment-water interface

Deleted: ,

Deleted: but forthcoming DNA analyses from these sediments should elucidate the role cable bacteria play in the SBB. Additionally, forthcoming sequential iron and sulfur extractions from SBB sediments should provide more information about the differences in early diagenesis throughout the basin.

Deleted: 4

1381 ~~Release of dissolved iron and phosphate from sediment below anoxic waters is a well-~~
1382 ~~documented phenomenon (e.g.,~~ (Mortimer, 1941; Van Cappellen and Ingall, 1994; Van De
1383 Velde et al., 2020; Noffke et al., 2012)) ~~and this phenomenon is seen in the SBB as well. As~~
1384 ~~postulated previously (Kuwabara et al., 1999), basin flushing oxidizes iron sulfides at the~~
1385 ~~sediment-water interface, providing ample substrate for microbial iron reduction once anoxia~~
1386 ~~returns. This iron reduction initiates high rates of Fe²⁺ release from SBB depocenter sediment~~
1387 ~~(Fig. 5). Iron reduction further releases iron-bound PO₄³⁻ (Mortimer, 1941) as seen by high~~
1388 ~~benthic fluxes of PO₄³⁻ at the depocenter (Fig. 5), although notably some of this PO₄³⁻ release is~~
1389 ~~likely attributed to organic matter degradation (Van Cappellen and Ingall, 1994). High benthic~~
1390 Fe²⁺ and PO₄³⁻ fluxes were also seen on the Peruvian shelf during transient anoxia (Noffke et al.,
1391 2012). The release of these solutes was interpreted to be sourced from a layer of reactive iron
1392 hydroxides existing near the sediment surface, likely established during a recent oxygenation
1393 event. Similar conditions, i.e., visibly oxidized (reddish) sediment laminae and a thin zone of
1394 iron reduction apparent from a peak in Fe²⁺ at the sediment-water interface, were found in
1395 sediment from the SBB depocenter. ~~Deeper in the persistently anoxic core of the Peruvian OMZ,~~
1396 ~~sediment appears to have little to no flux of Fe²⁺ and PO₄³⁻ into the bottom water (Noffke et al.,~~
1397 ~~2012). Here, iron at the sediment-water interface is hypothesized to be locked up in iron sulfides,~~
1398 ~~which are rarely re-oxidized due to persistent anoxia.~~
1399
1400 ~~In a different study from the Eastern Gotland Basin in the Baltic Sea, enhanced elemental fluxes~~
1401 ~~were observed during a decadal oxygen flushing event (Van De Velde et al., 2020), which was~~
1402 ~~attributed to enhanced elemental recycling, or cycles of mineral precipitation in the water column~~
1403 ~~followed by mineral dissolution once those minerals sink to the sediment. Notably, the iron flux~~

- Deleted: Benthic
- Deleted: flux out of
- Deleted: s
- Deleted: an
- Deleted: column has been
- Deleted: ation
- Deleted: anyof
- Deleted: upon basin flushing with oxygen likely encourages
- Deleted: when
- Deleted: occurs again
- Deleted: following later deoxygenation
- Deleted: causes
- Deleted: strong
- Deleted: and PO₄³⁻
- Deleted: fluxes out of
- Deleted: High
- Deleted: flux out
- Deleted: of anoxic sediment can be attributed to said iron reduction (Mortimer, 1941) as well as the release of
- Deleted: High porewater Fe²⁺ concentration (>100 μM) in the SBB D stations (Figs. 3L and V) indicate regions of prolific bacterial iron reduction in the sediment. As basin depth increases and oxygen concentration in the water decreases, the zone of iron reduction thins and is found closer to the sediment-water interface (Figs. 2 & 3). Further, high benthic fluxes of Fe²⁺ and PO₄³⁻ were observed in the transiently anoxic depocenter (Fig. 5).
- Deleted:
- Deleted: benthic
- Moved down [7]: These analogous observations highlight the importance of alternating redox conditions to establish high benthic iron fluxes.
- Deleted: E
- Deleted: due to transient deoxygenation has been
- Deleted: in the Eastern Gotland Basin of the Baltic Sea
- Deleted: where Fe and Mn flux are
- Deleted: ization
- Moved (insertion) [7]
- Deleted: and
- Deleted: (Van De Velde et al., 2020)
- Deleted: These analogous observations highlight the importance of alternating redox conditions to establish high benthic iron fluxes.
- Deleted: T

1447 observed in the Eastern Gotland Basin (max. 0.08 mmol m⁻² d⁻¹) (Van De Velde et al., 2020) was
1448 two orders of magnitude lower than the flux observed in the anoxic depocenter of the Santa
1449 Barbara Basin (max. 4.9 mmol m⁻² d⁻¹). It is further notable that benthic fluxes of PO₄³⁻ in the
1450 SBB depocenter were also an order of magnitude higher than fluxes in the Eastern Gotland
1451 Basin's hypoxic transition zone (3.6 vs. 0.23 mmol PO₄³⁻ m⁻² d⁻¹) - both of which contained
1452 GSOB mats, but while the SBB was anoxic and the Eastern Gotland Basin was hypoxic (Noffke
1453 et al., 2016). These differences in Fe²⁺ and PO₄³⁻ flux between the SBB and the Eastern Gotland
1454 Basin suggest that reoxidation of the sediment-water interface during basin flushing, as opposed
1455 to water-column-associated reoxidation, appears to encourage higher benthic iron fluxes.
1456
1457 Fe²⁺ and PO₄³⁻ flux from the SBB depocenter were also approximately five times higher (Fig. 5)
1458 compared to the anoxic Peruvian shelf (4.9 vs. 0.9 mmol Fe²⁺ m⁻² d⁻¹ and 3.6 vs. 0.8 mmol PO₄³⁻
1459 m⁻² d⁻¹, respectively) (Noffke et al., 2012). Based on Fe²⁺ profiles, the zone of iron reduction in
1460 Peruvian shelf sediments extended down to approx. 10 cm, while the zone appeared to be much
1461 shallower and narrower (less than the top 5 cm) in the SBB depocenter. These differences in
1462 magnitude of Fe²⁺ concentration and Fe²⁺ and PO₄³⁻ flux between the SBB depocenter and the
1463 Peruvian shelf could be attributed to differences in the recency and magnitude of reoxygenation
1464 events. The release of Fe²⁺ from sediment into the bottom water could create a buffer against
1465 reoxygenation in transiently deoxygenated systems, giving a competitive advantage to anaerobic
1466 benthic metabolisms (Dale et al., 2013; Wallmann et al., 2022). Additionally, both Fe²⁺ and
1467 PO₄³⁻ release from the SBB sediment could allow for higher rates of primary productivity if
1468 those constituents diffused into the photic zone (Robinson et al., 2022). The fate of Fe²⁺ and

Deleted: is

Deleted: core

Formatted: Superscript

Deleted: ting

Deleted:

Deleted:

Deleted: .

Deleted: (Raiswell and Canfield, 2012)

1476 PO_4^{3-} diffusing into SBB waters from the sediment-water interface is a focus of ongoing work
1477 within the basin.

1478
1479 **5 Conclusions**
1480

1481 This research expands upon the wealth of science already conducted in the SBB and other
1482 transiently deoxygenated environments by examining changes in benthic biogeochemistry
1483 promoted by the onset of anoxia. Our main interpretations are summarized in Fig. 7. We found
1484 that GSOB mats proliferate in the SBB where the bottom water is anoxic and nitrate
1485 concentrations are declining (Fig. 7, A- and depocenter stations). Nitrate uptake by SBB
1486 sediment is similar regardless of GSOB mat presence, but these mats appear to initiate a shift
1487 from denitrification to DNRA as the primary nitrate reduction pathway (Fig. 7, beginning at B-
1488 stations). The zone of sulfate reduction rises to the sediment-water interface where GSOB mats
1489 are present (Fig. 7, A-stations), possibly because the hyper-accumulation of nitrate into their
1490 intracellular vacuoles starves the environment of this more powerful electron acceptor. However,
1491 following the natural order of electron acceptor utilization (Boudreau and Jorgensen, 2001), iron
1492 oxides near the sediment-water interface must be exhausted before sulfate reduction can
1493 dominate surface sediments and GSOB mats can proliferate in the SBB (Fig. 7, depocenter
1494 stations). If anoxic events become longer and more frequent in the SBB because of global
1495 warming (see, e.g., (Qin et al., 2022; Stramma et al., 2008)), the iron oxide buffer built up in
1496 shallower basin depths could be exhausted, allowing for surface sulfate reduction and the
1497 proliferation of GSOB mats in shallower margins of the basin than currently seen. Further, the
1498 same transient deoxygenation that allows for these mats to re-establish themselves also allows for
1499 a high Fe^{2+} and PO_4^{3-} flux into the SBB water column. In order to fully understand the complex

Deleted:

Deleted:

Deleted: initiating a shift from primarily denitrification to an increase in DNRA. We conclude that GSOB mat proliferation in the SBB is confined to areas of the benthic environment with anoxic (though not completely anoxic) bottom water. The sulfate reduction zone is elevated to the surface sediments underneath these mats, but mat presence alone seems insufficient to change the depth of sulfate reduction

Deleted: While this nitrate uptake could help encourage the zone of sulfate reduction to migrate towards the surface

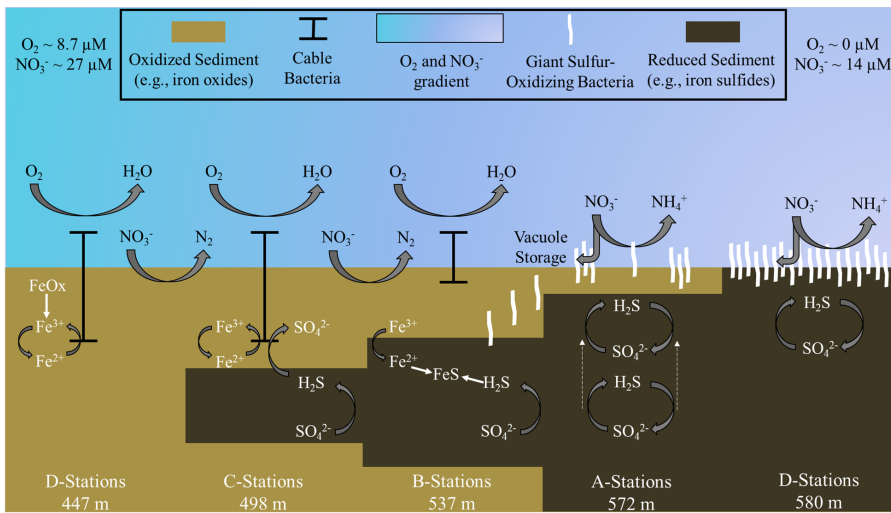
Deleted:

Deleted: We conclude suggest that changes in iron mineralogy, specifically the formation of an iron sulfide layer deeper in sediments, encourages the elevation of the sulfate reduction zone.

Deleted: flourish

1517 changes in the benthic environment in response to deoxygenation, genomic and molecular work
 1518 of the upper sediment community needs to be characterized. Overall, the insights gleaned from
 1519 this research will aid in the understanding of fundamental biogeochemical changes that occur
 1520 when marine environments become anoxic.

1521



1522 **Figure 7:** Schematic of biogeochemical processes in the Santa Barbara Basin along the depth gradients
 1523 studied in October/November 2019. Teal to Lavender gradient represents a decline in O_2 and NO_3^-
 1524 concentrations with basin depth. In the shallower, hypoxic basin (D-stations), denitrification and iron reduction
 1525 are dominant and reduced iron is rapidly re-oxidized in near-surface sediment by cable bacteria. Deeper in the
 1526 basin (A-stations and depocenter), nitrogen cycling shifts towards dissimilatory nitrate reduction to ammonia
 1527 (DNRA). Reduced iron combines with sulfide, produced by sulfate reduction, diffusing from deeper sediment
 1528 layers to form iron sulfides. As oxygen concentration approaches zero between the A-stations and the basin's
 1529 depocenter, giant sulfur-oxidizing bacteria hyper-accumulate nitrate in their intracellular vacuoles. Nitrate
 1530 removal combined with the exhaustion of available iron oxides in the near-surface sediments allows the zone
 1531 of sulfate reduction to migrate towards the surface (see dashed arrows at A-stations), providing the giant
 1532 sulfur-oxidizing bacteria with sufficient reduced sulfur to proliferate into thick, contiguous mats. Note: Figure
 1533 is not to scale, and processes are simplified to illustrate main concepts.

Deleted: is

Deleted:

1537 **Acknowledgements**

1538 We thank the captain, crew, and scientific party of the R/V Atlantis, and the crew of the ROV
1539 Jason for their technical and logistical support during the research expedition AT42-19. We also
1540 thank Q. Qin, E. Arrington, M. O’Beirne, A. Mazariegos, X. Moreno, A. Eastman, and K.
1541 Gosselin for assisting with shipboard analyses. We further thank M. Alisch from the Max-
1542 Planck-Institute in Bremen, Germany for DIC analyses. We thank G. Eickert-Grötzschel, V.
1543 Hübner, A. Niclas, I. Schröder, and C. Wigand from the Max-Planck-Institute in Bremen,
1544 Germany for constructing the microsensors. We acknowledge J. Matthews from the UC Davis
1545 Stable Isotope facility for assisting with solid phase analyses. Funding for this work was
1546 provided by the US National Science Foundation, NSF OCE-1756947 and OCE-1830033 (to
1547 DLV) and OCE-1829981 (to TT), and a [Simons Foundation Postdoctoral Fellowship in Marine](#)
1548 [Microbial Ecology \(No. 547606 to XP\)](#). Further support was provided by the Max Planck
1549 Society and the Alfred Wegener Institute for Polar and Marine Research.

1550

1551 **Data availability.**

1552 Biogeochemical data presented in this manuscript are accessible through the Biological &
1553 Chemical Oceanography Data Management Office (BCO-DMO) at the following landing pages:
1554 <https://www.bco-dmo.org/dataset/867007>; <https://www.bco-dmo.org/dataset/867113>;
1555 <https://www.bco-dmo.org/dataset/867221>; <https://www.bco-dmo.org/dataset/896706>

Deleted:).

1557 **Author contributions.**

1558 TT, DV, FK, NL, and JT designed the project. DJY, SK, JT, DR, and TT processed sediment
1559 cores at sea. DJY conducted geochemical analyses of sediment porewater and benthic flux
1560 chamber water. DJY prepared TOC and TON samples. DR and SK analyzed sediment porosity
1561 and density. TT and SK performed shipboard sulfate reduction incubations. DJY and DR
1562 conducted sulfate reduction analyses. DJY, NL, and JT transformed and interpreted ROV Jason
1563 data. FJ and FW operated BFC and microprofilers and analyzed associated data. XP conducted
1564 ¹⁵N experiments and analyses. All authors reviewed and edited the manuscript.

1565

1566 **Competing interests.**

1567 At least one of the (co-)authors is a member of the editorial board of Biogeosciences.

1568 **References**

- 1569
1570 Algar, C. K. and Vallino, J. J.: Predicting microbial nitrate reduction pathways in coastal sediments,
1571 *Aquatic Microbial Ecology*, 71, 223-238, 2014.
- 1572 An, S. and Gardner, W. S.: Dissimilatory nitrate reduction to ammonium (DNRA) as a nitrogen
1573 link, versus denitrification as a sink in a shallow estuary (Laguna Madre/Baffin Bay, Texas),
1574 *Marine Ecology Progress Series*, 237, 41-50, 2002.
- 1575 Bernhard, J. M., Visscher, P. T., and Bowser, S. S.: Submillimeter life positions of bacteria, protists,
1576 and metazoans in laminated sediments of the Santa Barbara Basin, *Limnology and*
1577 *Oceanography*, 48, 813-828, 2003.
- 1578 Bograd, S. J., Schwing, F. B., Castro, C. G., and Timothy, D. A.: Bottom water renewal in the Santa
1579 Barbara Basin, *Journal of Geophysical Research: Oceans*, 107, 9-1-9-9, 2002.
- 1580 Bonaglia, S., Nascimento, F. A., Bartoli, M., Klawonn, I., and Brüchert, V.: Meiofauna increases
1581 bacterial denitrification in marine sediments, *Nature communications*, 5, 5133, 2014.
- 1582 Boudreau, B. P. and Jorgensen, B. B.: The benthic boundary layer: Transport processes and
1583 biogeochemistry, 2001.
- 1584 Bourbonnais, A., Letscher, R. T., Bange, H. W., Echevin, V., Larkum, J., Mohn, J., Yoshida, N., and
1585 Altabet, M. A.: N₂O production and consumption from stable isotopic and concentration
1586 data in the Peruvian coastal upwelling system, *Global Biogeochemical Cycles*, 31, 678-698,
1587 2017.
- 1588 Bremner, J.: Biogenic sediments on the South West African continental margin, 1981.
- 1589 Brüchert, V., Jørgensen, B. B., Neumann, K., Riechmann, D., Schlösser, M., and Schulz, H.:
1590 Regulation of bacterial sulfate reduction and hydrogen sulfide fluxes in the central
1591 Namibian coastal upwelling zone, *Geochim. Cosmochim. Acta*, 67, 4505-4518, 2003.
- 1592 Caffrey, J. M., Bonaglia, S., and Conley, D. J.: Short exposure to oxygen and sulfide alter
1593 nitrification, denitrification, and DNRA activity in seasonally hypoxic estuarine sediments,
1594 *FEMS microbiology letters*, 366, fny288, 2019.
- 1595 California Cooperative Oceanic Fisheries Investigations: <https://www.calcofi.org/ccdata.html>, last
1596 Canfield, D. E.: Reactive iron in marine sediments, *Geochimica et cosmochimica acta*, 53, 619-
1597 632, 1989.
- 1598 Canfield, D. E., Stewart, F. J., Thamdrup, B., De Brabandere, L., Dalsgaard, T., Delong, E. F.,
1599 Revsbech, N. P., and Ulloa, O.: A cryptic sulfur cycle in oxygen-minimum-zone waters off
1600 the Chilean coast, *Science*, 330, 1375-1378, 2010.
- 1601 Charoenpong, C. N., Bristow, L. A., and Altabet, M. A.: A continuous flow isotope ratio mass
1602 spectrometry method for high precision determination of dissolved gas ratios and isotopic
1603 composition, *Limnology and Oceanography: Methods*, 12, 323-337, 2014.
- 1604 Cline, J. D.: Spectrophometric determination of hydrogen sulfide in natural waters, *Limnol.*
1605 *Oceanogr.*, 14, 454-458, 1969.
- 1606 Dale, A. W., Bertics, V. J., Treude, T., and Wallmann, K.: Modeling benthic-pelagic nutrient
1607 exchange processes and porewater distributions in a seasonally hypoxic sediment:
1608 evidence for massive phosphate release by *Beggiatoa*?, *Biogeosciences*, 10, 629-651,
1609 2013.
- 1610 Dale, A. W., Sommer, S., Lomnitz, U., Bourbonnais, A., and Wallmann, K.: Biological nitrate
1611 transport in sediments on the Peruvian margin mitigates benthic sulfide emissions and

Formatted: Indent: Left: -0.27 cm

1612 drives pelagic N loss during stagnation events, *Deep Sea Research Part I: Oceanographic*
 1613 *Research Papers*, 112, 123-136, 2016.

1614 Dale, A. W., Sommer, S., Ryabenko, E., Noffke, A., Bohlen, L., Wallmann, K., Stolpovsky, K.,
 1615 Greinert, J., and Pfannkuche, O.: Benthic nitrogen fluxes and fractionation of nitrate in the
 1616 Mauritanian oxygen minimum zone (Eastern Tropical North Atlantic), *Geochimica et*
 1617 *Cosmochimica Acta*, 134, 234-256, 2014.

1618 Dale, A. W., Sommer, S., Bohlen, L., Treude, T., Bertics, V. J., Bange, H. W., Pfannkuche, O.,
 1619 Schorp, T., Mattsdotter, M., and Wallmann, K.: Rates and regulation of nitrogen cycling in
 1620 seasonally hypoxic sediments during winter (Boknis Eck, SW Baltic Sea): Sensitivity to
 1621 environmental variables, *Estuar. Continent. Shelf Sci.*, 95, 14-28, 2011.

1622 Dale, A. W., Sommer, S., Lomnitz, U., Montes, I., Treude, T., Liebetau, V., Gier, J., Hensen, C.,
 1623 Dengler, M., Stolpovsky, K., Bryant, L. D., and Wallmann, K.: Organic carbon production,
 1624 mineralisation and preservation on the Peruvian margin, *Biogeosciences*, 12, 1537-1559,
 1625 2015.

1626 De Brabandere, L., Bonaglia, S., Kononets, M. Y., Viktorsson, L., Stigebrandt, A., Thamdrup, B.,
 1627 and Hall, P. O.: Oxygenation of an anoxic fjord basin strongly stimulates benthic
 1628 denitrification and DNRA, *Biogeochemistry*, 126, 131-152, 2015.

1629 Emery, K., Hülsemann, J., and Rodolfo, K.: Influence of turbidity currents upon basin waters,
 1630 *Limnology and Oceanography*, 7, 439-446, 1962.

1631 Emmer, E. and Thunell, R. C.: Nitrogen isotope variations in Santa Barbara Basin sediments:
 1632 Implications for denitrification in the eastern tropical North Pacific during the last 50,000
 1633 years, *Paleoceanography*, 15, 377-387, 2000.

1634 Fossing, H., Gallardo, V. A., Jørgensen, B. B., Hüttel, M., Nielsen, L. P., Schulz, H., Canfield, D. E.,
 1635 Forster, S., Glud, R. N., and Gundersen, J. K.: Concentration and transport of nitrate by the
 1636 mat-forming sulphur bacterium *Thioploca*, *Nature*, 374, 713-715, 1995a.

1637 Fossing, H., Gallardo, V. A., Jørgensen, B. B., Hüttel, M., Nielsen, L. P., Schulz, H., Canfield, D. E.,
 1638 Forster, S., Glud, R. N., Gundersen, J. K., Küver, J., Ramsing, N. B., Teske, A., Thamdrup, B.,
 1639 and Ulloa, O.: Concentration and transport of nitrate by the mat-forming sulphur
 1640 bacterium *Thioploca*, *Nature*, 374, 713-715, 1995b.

1641 García-Robledo, E., Corzo, A., and Papaspyrou, S.: A fast and direct spectrophotometric method
 1642 for the sequential determination of nitrate and nitrite at low concentrations in small
 1643 volumes, *Marine Chemistry*, 162, 30-36, 2014.

1644 Gier, J., Sommer, S., Löscher, C. R., Dale, A. W., Schmitz, R. A., and Treude, T.: Nitrogen fixation in
 1645 sediments along a depth transect through the Peruvian oxygen minimum zone,
 1646 *Biogeosciences*, 13, 4065-4080, 2016.

1647 Glud, R. N., Gundersen, J. K., and Ramsing, N. B.: Electrochemical and optical oxygen
 1648 microsensors for in situ measurements, in: *In situ monitoring of aquatic systems: Chemical analysis and speciation*, edited by: Buffle, J., and Horvai, G., Wiley, 2000.

1650 Goericke, R., Bograd, S. J., and Grundle, D. S.: Denitrification and flushing of the Santa Barbara
 1651 Basin bottom waters, *Deep Sea Research Part II: Topical Studies in Oceanography*, 112,
 1652 53-60, 2015.

1653 Grasshoff, K., Ehrhardt, M., and Kremling, K.: *Methods of seawater analysis*, Wiley-VCH Verlag
 1654 GmbH, Weinheim 1999.

1655 Gundersen, J. K. and Jørgensen, B. B.: Microstructure of diffusive boundary layers and the oxygen
 1656 uptake of the sea floor, *Nature*, 345, 604-607, 1990.
 1657 Hall, P. O. J. and Aller, R. C.: Rapid small-volume flow injection analysis for Σ CO₂ and NH₄⁺ in
 1658 marine and fresh waters, *Limnol. Oceanogr.*, 37, 1113-1119, 1992.
 1659 Hardison, A. K., Algar, C. K., Giblin, A. E., and Rich, J. J.: Influence of organic carbon and nitrate
 1660 loading on partitioning between dissimilatory nitrate reduction to ammonium (DNRA) and
 1661 N₂ production, *Geochimica et Cosmochimica Acta*, 164, 146-160, 2015.
 1662 Harris, D., Horwáth, W. R., and Van Kessel, C.: Acid fumigation of soils to remove carbonates prior
 1663 to total organic carbon or carbon-13 isotopic analysis, *Soil Science Society of America*
 1664 *Journal*, 65, 1853-1856, 2001.
 1665 Hermans, M., Lenstra, W. K., Hidalgo-Martinez, S., van Helmond, N. A., Witbaard, R., Meysman, F.
 1666 J., Gonzalez, S., and Slomp, C. P.: Abundance and biogeochemical impact of cable bacteria
 1667 in Baltic Sea sediments, *Environmental science & technology*, 53, 7494-7503, 2019.
 1668 Hossain, M., Bhattacharya, P., Frape, S. K., Jacks, G., Islam, M. M., Rahman, M. M., von Brömssen,
 1669 M., Hasan, M. A., and Ahmed, K. M.: Sediment color tool for targeting arsenic-safe
 1670 aquifers for the installation of shallow drinking water tubewells, *Science of the Total*
 1671 *Environment*, 493, 615-625, 2014.
 1672 Huettel, M., Forster, S., Kloser, S., and Fossing, H.: Vertical migration in the sediment-dwelling
 1673 sulfur bacteria *Thioploca* spp. in overcoming diffusion limitations, *Applied and*
 1674 *Environmental Microbiology*, 62, 1863-1872, 1996.
 1675 Hylén, A., Bonaglia, S., Robertson, E., Marzocchi, U., Kononets, M., and Hall, P. O.: Enhanced
 1676 benthic nitrous oxide and ammonium production after natural oxygenation of long-term
 1677 anoxic sediments, *Limnology and Oceanography*, 67, 419-433, 2022.
 1678 Høgslund, S., Revsbech, N. P., Kuenen, J. G., Jørgensen, B. B., Gallardo, V. A., Vossenberg, J. v. d.,
 1679 Nielsen, J. L., Holmkvist, L., Arning, E. T., and Nielsen, L. P.: Physiology and behaviour of
 1680 marine *Thioploca*, *The ISME journal*, 3, 647-657, 2009.
 1681 Jensen, M. M., Lam, P., Revsbech, N. P., Nagel, B., Gaye, B., Jetten, M. S., and Kuypers, M. M.:
 1682 Intensive nitrogen loss over the Omani Shelf due to anammox coupled with dissimilatory
 1683 nitrite reduction to ammonium, *The ISME journal*, 5, 1660-1670, 2011.
 1684 Jeroschewsky, P., Steuckart, C., and Kuehl, M.: An amperometric microsensor for the
 1685 determination of H₂S in aquatic environments, *Anal. Chem.*, 68, 4351-4357, 1996.
 1686 Jørgensen, B.: Distribution of colorless sulfur bacteria (*Beggiatoa* spp.) in a coastal marine
 1687 sediment, *Marine Biology*, 41, 19-28, 1977.
 1688 Jørgensen, B. B.: A comparison of methods for the quantification of bacterial sulphate reduction
 1689 in coastal marine sediments: I. Measurements with radiotracer techniques, *Geomicrobiol.*
 1690 *J.*, 1, 11-27, 1978.
 1691 Jørgensen, B. B. and Nelson, D. C.: Sulfide oxidation in marine sediments: Geochemistry meets
 1692 microbiology, *Geological Society of America, Special Paper* 379, 63-81, 2004.
 1693 Kallmeyer, J., Ferdelman, T. G., Weber, A., Fossing, H., and Jørgensen, B. B.: A cold chromium
 1694 distillation procedure for radiolabeled sulfide applied to sulfate reduction measurements,
 1695 *Limnol. Oceanogr. Methods*, 2, 171-180, 2004.

1696 Kamp, A., de Beer, D., Nitsch, J. L., Lavik, G., and Stief, P.: Diatoms respire nitrate to survive dark
1697 and anoxic conditions, *Proceedings of the National Academy of Sciences*, 108, 5649-5654,
1698 2011.

1699 Kessler, A. J., Wawryk, M., Marzocchi, U., Roberts, K. L., Wong, W. W., Risgaard-Petersen, N.,
1700 Meysman, F. J., Glud, R. N., and Cook, P. L.: Cable bacteria promote DNRA through iron
1701 sulfide dissolution, *Limnology and Oceanography*, 64, 1228-1238, 2019.

1702 Kjeldsen, K. U., Schreiber, L., Thorup, C. A., Boesen, T., Bjerg, J. T., Yang, T., Dueholm, M. S.,
1703 Larsen, S., Risgaard-Petersen, N., and Nierychlo, M.: On the evolution and physiology of
1704 cable bacteria, *Proceedings of the National Academy of Sciences*, 116, 19116-19125,
1705 2019.

1706 Kononets, M., Tengberg, A., Nilsson, M., Ekeröth, N., Hylén, A., Robertson, E. K., Van De Velde, S.,
1707 Bonaglia, S., Rütting, T., and Blomqvist, S.: In situ incubations with the Gothenburg
1708 benthic chamber landers: Applications and quality control, *Journal of Marine Systems*,
1709 214, 103475, 2021.

1710 Kraft, B., Tegetmeyer, H. E., Sharma, R., Klotz, M. G., Ferdelman, T. G., Hettich, R. L., Geelhoed, J.
1711 S., and Strous, M.: The environmental controls that govern the end product of bacterial
1712 nitrate respiration, *Science*, 345, 676-679, 2014.

1713 Kuwabara, J. S., van Geen, A., McCorkle, D. C., and Bernhard, J. M.: Dissolved sulfide distributions
1714 in the water column and sediment pore waters of the Santa Barbara Basin, *Geochimica et*
1715 *Cosmochimica Acta*, 63, 2199-2209, 1999.

1716 Levin, L. A., Gutierrez, D., Rathburn, A. E., Neira, C., Sellanes, J., Munoz, P., Gallardo, V. A., and
1717 Salamance, M.: Benthic processes on the Peru margin: a transect across the oxygen
1718 minimum zone during the 1997-98 El Niño, *Prog. Oceanog.*, 53, 1-27, 2002.

1719 Marchant, H. K., Lavik, G., Holtappels, M., and Kuypers, M. M.: The fate of nitrate in intertidal
1720 permeable sediments, *PloS one*, 9, e104517, 2014.

1721 Marzocchi, U., Bonaglia, S., van de Velde, S., Hall, P. O., Schramm, A., Risgaard-Petersen, N., and
1722 Meysman, F. J.: Transient bottom water oxygenation creates a niche for cable bacteria in
1723 long-term anoxic sediments of the Eastern Gotland Basin, *Environmental microbiology*,
1724 20, 3031-3041, 2018.

1725 Marzocchi, U., Trojan, D., Larsen, S., Louise Meyer, R., Peter Revsbech, N., Schramm, A., Peter
1726 Nielsen, L., and Risgaard-Petersen, N.: Electric coupling between distant nitrate reduction
1727 and sulfide oxidation in marine sediment, *The ISME journal*, 8, 1682-1690, 2014.

1728 Middelburg, J. and Levin, L.: Coastal hypoxia and sediment biogeochemistry, *Biogeosciences*, 6,
1729 1273-1293, 2009.

1730 Mortimer, C. H.: The exchange of dissolved substances between mud and water in lakes, *Journal*
1731 *of ecology*, 29, 280-329, 1941.

1732 Mosch, T., Sommer, S., Dengler, M., Noffke, A., Bohlen, L., Pfannkuche, O., Liebetrau, V., and
1733 Wallmann, K.: Factors influencing the distribution of epibenthic megafauna across the
1734 Peruvian oxygen minimum zone, *Deep Sea Research Part I: Oceanographic Research*
1735 *Papers*, 68, 123-135, 2012.

1736 Mußmann, M., Schulz, H. N., Strotmann, B., Kjær, T., Nielsen, L. P., Rosselló-Mora, R. A., Amann,
1737 R. I., and Jørgensen, B. B.: Phylogeny and distribution of nitrate-storing *Beggiatoa* spp. in
1738 coastal marine sediments, *Environmental Microbiology*, 5, 523-533, 2003.

- 1739 Myhre, S. E., Pak, D., Borreggine, M., Kennett, J. P., Nicholson, C., Hill, T. M., and Deutsch, C.:
 1740 Oxygen minimum zone biotic baseline transects for paleoceanographic reconstructions in
 1741 Santa Barbara Basin, CA, Deep Sea Research Part II: Topical Studies in Oceanography, 150,
 1742 118-131, 2018.
- 1743 Naik, R., Naqvi, S., and Araujo, J.: Anaerobic carbon mineralisation through sulphate reduction in
 1744 the inner shelf sediments of eastern Arabian Sea, Estuaries and Coasts, 40, 134-144, 2017.
- 1745 Noffke, A., Sommer, S., Dale, A., Hall, P., and Pfannkuche, O.: Benthic nutrient fluxes in the
 1746 Eastern Gotland Basin (Baltic Sea) with particular focus on microbial mat ecosystems,
 1747 Journal of Marine Systems, 158, 1-12, 2016.
- 1748 Noffke, A., Hensen, C., Sommer, S., Scholz, F., Bohlen, L., Mosch, T., Graco, M., and Wallmann, K.:
 1749 Benthic iron and phosphorus fluxes across the Peruvian oxygen minimum zone, Limnol.
 1750 Oceanogr., 57, 851-867, 2012.
- 1751 Pavlova, G. Y., Tishchenko, P. Y., Volkova, T., Dickson, A., and Wallmann, K.: Intercalibration of
 1752 Bruevich's method to determine the total alkalinity in seawater, Oceanology, 48, 438-443,
 1753 2008.
- 1754 Peng, X., Ji, Q., Angell, J. H., Kearns, P. J., Yang, H. J., Bowen, J. L., and Ward, B. B.: Long-term
 1755 fertilization alters the relative importance of nitrate reduction pathways in salt marsh
 1756 sediments, Journal of Geophysical Research: Biogeosciences, 121, 2082-2095, 2016.
- 1757 Peng, X., Yousavich, D. J., Bourbonnais, A., Wenzhoefer, F., Janssen, F., Treude, T., and Valentine,
 1758 D. L.: The fate of fixed nitrogen in Santa Barbara Basin sediments during seasonal anoxia,
 1759 EGUosphere, 2023, 1-26, 2023.
- 1760 Pfeffer, C., Larsen, S., Song, J., Dong, M., Besenbacher, F., Meyer, R. L., Kjeldsen, K. U., Schreiber,
 1761 L., Gorby, Y. A., and El-Naggar, M. Y.: Filamentous bacteria transport electrons over
 1762 centimetre distances, Nature, 491, 218-221, 2012.
- 1763 Plass, A., Schlosser, C., Sommer, S., Dale, A. W., Achterberg, E. P., and Scholz, F.: The control of
 1764 hydrogen sulfide on benthic iron and cadmium fluxes in the oxygen minimum zone off
 1765 Peru, Biogeosciences, 17, 3685-3704, 2020.
- 1766 Porubsky, W., Weston, N., and Joye, S.: Benthic metabolism and the fate of dissolved inorganic
 1767 nitrogen in intertidal sediments, Estuarine, Coastal and Shelf Science, 83, 392-402, 2009.
- 1768 Preisler, A., De Beer, D., Lichtschlag, A., Lavik, G., Boetius, A., and Jørgensen, B. B.: Biological and
 1769 chemical sulfide oxidation in a Beggiatoa inhabited marine sediment, ISME Journal, 341-
 1770 351, 2007.
- 1771 Prokopenko, M., Hammond, D., Berelson, W., Bernhard, J., Stott, L., and Douglas, R.: Nitrogen
 1772 cycling in the sediments of Santa Barbara basin and Eastern Subtropical North Pacific:
 1773 Nitrogen isotopes, diagenesis and possible chemosymbiosis between two lithotrophs
 1774 (Thioploca and Anammox)—“riding on a glider”, Earth and Planetary Science Letters, 242,
 1775 186-204, 2006.
- 1776 Qin, Q., Kinnaman, F. S., Gosselin, K. M., Liu, N., Treude, T., and Valentine, D. L.: Seasonality of
 1777 Water Column Methane Oxidation and Deoxygenation in a Dynamic Marine Environment,
 1778 Geochimica et Cosmochimica Acta, 2022.
- 1779 Raiswell, R. and Canfield, D. E.: The iron biogeochemical cycle past and present, Geochemical
 1780 perspectives, 1, 1-2, 2012.

- 1781 Reimers, C. E., Ruttenberg, K. C., Canfield, D. E., Christiansen, M. B., and Martin, J. B.: Porewater
 1782 pH and authigenic phases formed in the uppermost sediments of Santa Barbara Basin,
 1783 *Geochim. Cosmochim. Acta*, 60, 4037-4057, 1996a.
- 1784 Reimers, C. E., Ruttenberg, K. C., Canfield, D. E., Christiansen, M. B., and Martin, J. B.: Porewater
 1785 pH and authigenic phases formed in the uppermost sediments of the Santa Barbara Basin,
 1786 *Geochimica et Cosmochimica Acta*, 60, 4037-4057, 1996b.
- 1787 Revsbech, N. P. and Jørgensen, B. B.: Microelectrodes: their use in microbial ecology, in: *Adv.*
 1788 *Microb. Ecol.*, edited by: Marshall, K. C., Plenum, New York, 293-352, 1986.
- 1789 Robinson, D. M., Pham, A. L., Yousavich, D. J., Janssen, F., Wenzhöfer, F., Arrington, E. C.,
 1790 Gosselin, K. M., Sandoval-Belmar, M., Mar, M., and Valentine, D. L.: Iron "Ore" Nothing:
 1791 Benthic iron fluxes from the oxygen-deficient Santa Barbara Basin enhance phytoplankton
 1792 productivity in surface waters, *Biogeosciences Discussions*, 1-36, 2022.
- 1793 Sayama, M.: Presence of nitrate-accumulating sulfur bacteria and their influence on nitrogen
 1794 cycling in a shallow coastal marine sediment, *Applied and Environmental Microbiology*,
 1795 67, 3481-3487, 2001.
- 1796 Schauer, R., Risgaard-Petersen, N., Kjeldsen, K. U., Tataru Bjerg, J. J., B Jørgensen, B., Schramm,
 1797 A., and Nielsen, L. P.: Succession of cable bacteria and electric currents in marine
 1798 sediment, *The ISME journal*, 8, 1314-1322, 2014.
- 1799 Schroller-Lomnitz, U., Hensen, C., Dale, A. W., Scholz, F., Clemens, D., Sommer, S., Noffke, A., and
 1800 Wallmann, K.: Dissolved benthic phosphate, iron and carbon fluxes in the Mauritanian
 1801 upwelling system and implications for ongoing deoxygenation, *Deep Sea Research Part I:*
 1802 *Oceanographic Research Papers*, 143, 70-84, 2019.
- 1803 Schulz, H. N. and Schulz, H. D.: Large sulfur bacteria and the formation of phosphorite, *Science*,
 1804 307, 416-418, 2005.
- 1805 Schulz, H. N., Jørgensen, B. B., Fossing, H. A., and Ramsing, N. B.: Community structure of
 1806 filamentous, sheath-building sulfur bacteria, *Thioploca* spp., off the coast of Chile, *Applied*
 1807 *and Environmental Microbiology*, 62, 1855-1862, 1996.
- 1808 Schulz, H. N., Brinkhoff, T., Ferdelman, T. G., Hernández Mariné, M., Teske, A., and Jørgensen, B.
 1809 B.: Dense populations of a giant sulfur bacterium in Namibian shelf sediments, *Science*,
 1810 284, 493-495, 1999.
- 1811 Seitaj, D., Schauer, R., Sulu-Gambari, F., Hidalgo-Martinez, S., Malkin, S. Y., Burdorf, L. D., Slomp,
 1812 C. P., and Meysman, F. J.: Cable bacteria generate a firewall against euxinia in seasonally
 1813 hypoxic basins, *Proceedings of the National Academy of Sciences*, 112, 13278-13283,
 1814 2015.
- 1815 Sholkovitz, E.: Interstitial water chemistry of the Santa Barbara Basin sediments, *Geochimica et*
 1816 *Cosmochimica Acta*, 37, 2043-2073, 1973.
- 1817 Sholkovitz, E. R. and Gieskes, J. M.: A PHYSICAL-CHEMICAL STUDY OF THE FLUSHING OF THE
 1818 SANTA BARBARA BASIN 1, *Limnology and Oceanography*, 16, 479-489, 1971.
- 1819 Sigman, D. M., Robinson, R., Knapp, A., Van Geen, A., McCorkle, D., Brandes, J., and Thunell, R.:
 1820 Distinguishing between water column and sedimentary denitrification in the Santa
 1821 Barbara Basin using the stable isotopes of nitrate, *Geochemistry, Geophysics,*
 1822 *Geosystems*, 4, 2003.

- 1823 Sommer, S., Gier, J., Treude, T., Lomnitz, U., Dengler, M., Cardich, J., and Dale, A. W.: Depletion of
1824 oxygen, nitrate and nitrite in the Peruvian oxygen minimum zone cause an imbalance of
1825 benthic nitrogen fluxes, *Deep-Sea Res. I*, 112, 113–122, 2016.
- 1826 Stramma, L., Johnson, G. C., Sprintall, J., and Mohrholz, V.: Expanding oxygen-minimum zones in
1827 the tropical oceans, *Science*, 320, 655-658, 2008.
- 1828 Sverdrup, H. and Allen, W.: Distribution of diatoms in relation to the character of water masses
1829 and currents off Southern California in 1938, *J. mar. Res*, 2, 131-144, 1939.
- 1830 Thunell, R. C.: Particle fluxes in a coastal upwelling zone: sediment trap results from Santa
1831 Barbara Basin, California, *Deep Sea Research Part II: Topical Studies in Oceanography*, 45,
1832 1863-1884, 1998.
- 1833 Tiedje, J. M., Sexstone, A. J., Myrold, D. D., and Robinson, J. A.: Denitrification: ecological niches,
1834 competition and survival, *Antonie van Leeuwenhoek*, 48, 569-583, 1983.
- 1835 Treude, T.: Biogeochemical reactions in marine sediments underlying anoxic water bodies, in:
1836 *Anoxia: Paleontological Strategies and Evidence for Eukaryote Survival*, edited by:
1837 Altenbach, A., Bernhard, J., and Seckbach, J., *Cellular Origins, Life in Extreme Habitats and*
1838 *Astrobiology (COLE) Book Series*, Springer, Dordrecht, 18-38, 2011.
- 1839 Treude, T., Hamdan, L. J., Lemieux, S., Dale, A. W., and Sommer, S.: Rapid sulfur cycling in
1840 sediments from the Peruvian oxygen minimum zone featuring simultaneous sulfate
1841 reduction and sulfide oxidation, *Limnology and Oceanography*, 66, 2661-2671, 2021.
- 1842 Treude, T., Smith, C. R., Wenzhoefer, F., Carney, E., Bernardino, A. F., Hannides, A. K., Krueger,
1843 M., and Boetius, A.: Biogeochemistry of a deep-sea whale fall: sulfate reduction, sulfide
1844 efflux and methanogenesis, *Mar. Ecol. Prog. Ser.*, 382, 1-21, 2009.
- 1845 Valentine, D. L., Fisher, G. B., Pizarro, O., Kaiser, C. L., Yoerger, D., Breier, J. A., and Tarn, J.:
1846 Autonomous marine robotic technology reveals an expansive benthic bacterial
1847 community relevant to regional nitrogen biogeochemistry, *Environmental science &*
1848 *technology*, 50, 11057-11065, 2016.
- 1849 Van Cappellen, P. and Ingall, E. D.: Benthic phosphorus regeneration, net primary production,
1850 and ocean anoxia: A model of the coupled marine biogeochemical cycles of carbon and
1851 phosphorus, *Paleoceanography*, 9, 677-692, 1994.
- 1852 Van De Velde, S., Lesven, L., Burdorf, L. D., Hidalgo-Martinez, S., Geelhoed, J. S., Van Rijswijk, P.,
1853 Gao, Y., and Meysman, F. J.: The impact of electrogenic sulfur oxidation on the
1854 biogeochemistry of coastal sediments: A field study, *Geochimica et Cosmochimica Acta*,
1855 194, 211-232, 2016.
- 1856 van de Velde, S. J., Hylén, A., Eriksson, M., James, R. K., Kononets, M. Y., Robertson, E. K., and
1857 Hall, P. O.: Exceptionally high respiration rates in the reactive surface layer of sediments
1858 underlying oxygen-deficient bottom waters, *Proceedings of the Royal Society A*, 479,
1859 20230189, 2023.
- 1860 van de Velde, S. J., Hylén, A., Kononets, M., Marzocchi, U., Leermakers, M., Choumiline, K., Hall,
1861 P. O., and Meysman, F. J.: Elevated sedimentary removal of Fe, Mn, and trace elements
1862 following a transient oxygenation event in the Eastern Gotland Basin, central Baltic Sea,
1863 *Geochimica et Cosmochimica Acta*, 271, 16-32, 2020.
- 1864 Wallmann, K., José, Y. S., Hopwood, M. J., Somes, C. J., Dale, A. W., Scholz, F., Achterberg, E. P.,
1865 and Oschlies, A.: Biogeochemical feedbacks may amplify ongoing and future ocean

1866 deoxygenation: a case study from the Peruvian oxygen minimum zone, *Biogeochemistry*,
1867 159, 45-67, 2022.

1868 Ward, B., Devol, A., Rich, J., Chang, B., Bulow, S., Naik, H., Pratihary, A., and Jayakumar, A.:
1869 Denitrification as the dominant nitrogen loss process in the Arabian Sea, *Nature*, 461, 78-
1870 81, 2009.

1871 Xuefeng Peng, D. J., Yousavich, A. B., Frank Wenzhoefer,, Felix Jan b en , T., and Valentine, T. a.
1872 D. L.: The fate of fixed nitrogen in Santa Barbara Basin sediments
1873 during seasonal anoxia, 2023.

1874 Zhang, L., Altabet, M. A., Wu, T., and Hadas, O.: Sensitive measurement of NH₄⁺ ¹⁵N/¹⁴N
1875 ($\delta^{15}\text{NH}_4^+$) at natural abundance levels in fresh and saltwaters, *Analytical Chemistry*, 79,
1876 5297-5303, 2007.

1877 Zopfi, J., Kjær, T., Nielsen, L. P., and Jørgensen, B. B.: Ecology of *Thioploca* spp.: nitrate and sulfur
1878 storage in relation to chemical microgradients and influence of *Thioploca* spp. on the
1879 sedimentary nitrogen cycle, *Applied and Environmental Microbiology*, 67, 5530-5537,
1880 2001.

1881
1882

Page 33: [1] Deleted David Yousavich 10/4/23 4:32:00 PM

Page 33: [2] Deleted David Yousavich 10/4/23 2:32:00 PM

Page 33: [3] Deleted David Yousavich 10/4/23 4:29:00 PM

Page 33: [4] Deleted David Yousavich 10/4/23 4:29:00 PM

Page 33: [5] Deleted David Yousavich 10/4/23 4:29:00 PM